A compendium of current developments on polysaccharide and protein-based microneedles

Daniela F.S. Fonseca, Carla Vilela, Armando J.D. Silvestre, Carmen S.R. Freire

PII: S0141-8130(19)31489-8
DOI: https://doi.org/10.1016/j.ijbiomac.2019.04.163
Reference: BIOMAC 12239

To appear in: *International Journal of Biological Macromolecules*

Received date: 26 February 2019
Revised date: 21 April 2019
Accepted date: 22 April 2019

Please cite this article as: D.F.S. Fonseca, C. Vilela, A.J.D. Silvestre, et al., A compendium of current developments on polysaccharide and protein-based microneedles, International Journal of Biological Macromolecules, https://doi.org/10.1016/j.ijbiomac.2019.04.163

A compendium of current developments on polysaccharide and protein-based microneedles

Daniela F. S. Fonseca, Carla Vilela, Armando J. D. Silvestre and Carmen S. R. Freire*

CICECO – Aveiro Institute of Materials, Department of Chemistry, University of Aveiro, 3810-193 Aveiro, Portugal.

***Corresponding Author**

Carmen S. R. Freire

CICECO – Aveiro Institute of Materials, Department of Chemistry, University of Aveiro, 3810-193 Aveiro, Portugal

Email: cfreire@ua.pt.

Abstract

Microneedles (MNs), *i.e.* minimally invasive three-dimensional microstructures that penetrate the *stratum corneum* inducing relatively little or no pain, have been studied as appealing therapeutic vehicles for transdermal drug delivery (TDD). Over the last years, the fabrication of MNs using biopolymers, such as polysaccharides and proteins, has sparked the imagination of scientists due to their recognized biocompatibility, biodegradability, ease of fabrication and sustainable character. Owing to their wide range of functional groups, polysaccharides and proteins enable the design and preparation of materials with tunable properties and functionalities. Therefore, these biopolymer-based MNs take a revolutionary step offering great potential not only in drug

administration, but also in sensing and response to physiological stimuli. In this review, a critical and comprehensive overview of the polysaccharides and proteins employed in the design and engineering of MNs will be given. The strategies adopted for their preparation, their advantages and disadvantages will be also detailed. In addition, the potential and challenges of using these matrices to deliver drugs, vaccines and other molecules will be discussed. Finally, this appraisal ends with a perspective on the possibilities and challenges in research and development of polysaccharide and protein MNs, envisioning the future advances and clinical translation of these platforms as the next generation of drug delivery systems

Keywords: microneedles, biopolymers, polysaccharides, proteins, transdermal application.

1. Introduction

During the past few decades, we have witnessed an enormous progress in the research, development and improvement of drug delivery systems (DDS) [1–3]. The technological advances of this burgeoning field emerged as optimized formulations or delivery devices, aiming to enhance the therapeutic efficacy of the different pharmacological agents, either biotherapeutics (*e.g.*, insulin and vaccines) or drugs (*e.g.*, diclofenac and ibuprofen) [3,4]. Notably, considering that the therapeutic efficiency relies on the administration route, the focus is to overcome the challenges of conventional drug delivery (DD). The most common limitations are the pharmaceutical's degradation in the gastrointestinal tract in oral administration, and the poor patient compliance of parenteral injections [1,2,5]. Therefore, the field of DD is driving research towards the development of easy-to-use systems, with good patient compliance, a reduced frequency of dosing and self-administration at the point-of-care, with lower therapy costs and reduced environmental impact [6–10].

Among the different DDS, transdermal drug delivery (TDD) aiming at delivering pharmaceuticals through skin, has attracted a lot of attention. From a global perspective, the transdermal route offers key benefits such as targeted delivery and lower systemic exposure and toxicity, because drugs avoid first-pass metabolism, gastrointestinal degradation and food-drug interactions, thus improving their bioavailability [11–13]. Furthermore, the simple and painless self-application of TDD systems, coupled with their easy storage and transportation, makes them particularly relevant for health care in developing countries [6,8,14]. Regardless of these features, TDD success is hindered by the barrier function provided by skin, which due to its complex and multi-layered cellular architecture, limits DD efficiency [15]. In general, suitable candidates for TDD are molecules with potent pharmacological activity, low molecular weight (MW <400 Da, ideally),

balanced lipophilicity (log *P*(octanol-water partition coefficient) ideally around 2 to 3) and a measurable solubility both in oil and water [16]. Hence, TDD is restricted to a narrow range of pharmaceuticals, as a result of the difficulty of finding formulations with appropriate physicochemical properties to passively permeate through skin [6,13].

To address these limitations and enable successful transdermal delivery of different pharmaceuticals, a rather-novel strategy involves using microneedles (MNs) [17–20]. These DDS are three-dimensional micron-sized needles placed on the underside of a patch, designed to combine the advantages of both hypodermic needles and transdermal patches as illustrated in Figure 1 [21].

Throughout the history of MNs fabrication, a wide range of materials has been reported. The first MNs were fabricated using silicon [22–24],metals (*e.g.*, titanium [25] and stainless steel [26]), ceramics [27] and glass [28]. Nevertheless, polymers are nowadays playing a central role in the preparation of MNs [18,29]. This large and versatile class of materials can be tailored with a great variety of structures and hence, physical and biological functions to meet specific needs [30–32]. In this vein, polymers are considered one of the cornerstones for biomedical applications [32–34]. Currently, as a result of the general concern for sustainability, biopolymers, in particular polysaccharides and proteins, are receiving unprecedented attention over the synthetic polymers in the fabrication of MNs. This is due to their biocompatibility and low immunogenicity, biomimetic features, ability to enhance drug pharmacokinetics, abundance and renewable character [3,32,35–37]. The panoply of biopolymers available in nature has allowed the fabrication of MNs with unique characteristics [38–40], and from this perspective, the infinite opportunities of fabricating sophisticated biopolymer-based MNs are only limited by our imagination.

At the moment, there are several excellent general reviews on the subject of DD using MNs [17,18,41–45]. For instance, Larrañeta *et al*. [43] and Rejinold *et al*. [17] reviewed the composition and properties of MNs, as well as their applications and clinical translation. On the other hand, Ita *et al*. [42] has contributed with insights into the fabrication of MNs and outcomes of clinical trials, and recently shed light on the general features of ceramic and hollow MNs [41]. Additionally, their use in biosensing applications was reviewed by Cahill and O'Cearbhaill [44]. Attention has also been placed on polymeric MNs and Wang *et al* [18] provided a guideline regarding the fabrication methods and applications of polymeric MNs, either of synthetic or natural origin. On a different perspective, Ye *et al*. [45] focused particularly on the role of polymeric MNs for the transdermal delivery of proteins.

To the best of our knowledge, no comprehensive appraisals devoted exclusively to biopolymeric MNs have been published to date. Therefore, considering the current relevance and magnitude of biopolymers and biopolymeric-based materials, this review addresses the preparation and challenges of using polysaccharide and protein-based MNs for DD purposes. Herein, we will first provide a brief overview of the general characteristics and DD strategies of MNs. Then, a discussion about the potential and challenges of using polysaccharide and protein-based MNs to deliver drugs, vaccines and other molecules will be given. Finally, a critical overview on the future and clinical translation of polysaccharide and protein-based MNs will be highlighted.

2. Fundamentals of microneedles

2.1. Definition and characteristics

MNs, first conceptualized in 1976 [46], take the form of transdermal patches with microscale protrusions designed to disrupt the *stratum corneum (SC*) of the skin and other epithelial tissues,

creating microconduits through which external molecules can passively diffuse (Figure 1) [47–49].

Typically, MNs have from 25 to 2000 μm in length [50], small enough to avoid stimulation of peripheral nerve fibers or puncture the blood vessels. Upon application of MNs, DD efficiency can be dramatically enhanced, and the types of drugs transported *via* transdermal route can be significantly diversified [17,18,43]. In 1998, Henry *et al*. [47] reported the successful fabrication of solid silicon MNs for TDD of calcein (hydrophilic drug of 622.5 Da), showing for the first time that the *in vitro* permeability of human skin could be increased by up to 4 orders of magnitude, after pierced by 150 μm long needles.

Conceptually, the success of MNs results from combining the advantages of traditional TDD systems with the targeting of conventional hypodermic needles. Some key drivers for this enduring success are minimal invasiveness, low pain, self-administration, easy disposal and the ability to increase transcutaneous flux of pharmaceuticals [17,18,43,45]. In contrast, the creation of microscopic pores that lead to hypersensitivity reactions, delayed onset, reliable dosing and the potential for misuse, are some of the concerns regarding these DD devices [51]. In general, MNs can be classified accordingly to their structure (Figure 2 (A)), body shape (Figure 2 (B)) and tip shape (Figure 2 (C)) [43,52].

MNs are fabricated into two basic designs, the in-plane (Figure 2 (A)a) and out-of-plane (Figure 2 (A)b) [43,52]. The needles of in-plane MNs are parallel to the fabrication surface, whereas the out-of-plane MNs arise perpendicular to the baseplate. In addition, the out-of-plane MNs can be classified as hollow (Figure 2 (B)a) or solid (Figure 2 (B)b) shape MNs, with different geometries, such as cylindrical (Figure 2 (C)a), tapered tip (Figure 2 (C)b), conical (Figure 2 (C)c), square base or pyramidal (Figure 2 (C)d) and pentagonal-base conical tip (Figure 2 (C)e) [52].

2.2. Drug delivery strategies

The delivery of therapeutic agents using MNs is typically described according to five types of systems and the associated patterns of DD. Specifically, MNs can be classified as solid (Figure 3 (a)), coated (Figure 3 (b)), dissolving (Figure 3 (c)), hollow (Figure 3 (d)) and hydrogel-forming MNs (Figure 3 (e)) [43].

Solid, coated and hollow MNs can be fabricated using silicon [22–24], metals and alloys (*e.g.*, titanium [25], stainless steel [26], palladium, palladium-cobalt alloys and nickel [53,54]), ceramics (*e.g.*, ceramic oxides such as alumina, zirconia and fused silica [27]), glass [28,55] and polymers (*e.g.*, polyvinylpyrrolidone [56], poly(vinyl alcohol) (PVA) [57], poly(γ-glutamic acid) [58], chitosan (CS) [40,59,60], hyaluronic acid (HA) [61–65], among others [66–71]. Dissolving MNs can be fabricated using sugars (*e.g.*, maltose, trehalose and sucrose [72,73]) or polymers [56,57,66,74–77] whereas hydrogel-forming MNs are prepared using polymers [17–19,43].

Solid MNs (Figure 3 (a)), employed in the so-called 'poke with patch' approach, were developed as a 1st generation transcutaneous system [78,79]. First, MNs are applied to skin to create transient pores in the *SC*. Then, conventional drug formulations like transdermal patches, ointments, creams, gels or lotions are applied, and the permeation occurs *via* passive diffusion [78–80].

Coated MNs (Figure 3 (b)) rely on the 'coat and poke' strategy which consists in coating the arrays with therapeutic formulations that are deposited after skin insertion [81]. The pharmaceutical formulations are applied alone or combined in polymeric matrices, usually by dip coating [81,82]. More recently, scientists have explored additive manufacturing, namely by layer-by-layer (LbL) approaches to deposit therapeutic agents in different layers, using polyelectrolyte solutions or polymeric nanocapsules [83,84]. Coated MNs may be an alternative for vaccination purposes or

the delivery of potent drugs, but are not suitable for applications requiring high drug doses due to the restricted amounts that can be coated onto the finite surface area of the MNs [81].

Dissolving MNs (Figure 3 (c)) is an umbrella term used to describe dissolving or degradable matrices. The DD strategy is based upon the 'poke and release' approach. In brief, the array is inserted into the skin and after contacting with the interstitial skin fluid (ISF) the needle structure releases its cargo [12,78]. The pharmaceutical agents can be introduced in the tip of the needle, in the whole needle structure as part of matrix and also encapsulated in particles [17,85]. The main limitation of using dissolvable MNs is the deposition of material into skin if they are used on a regular basis, which possibly can make these devices undesirable [86].

Hollow MNs (Figure 3 (d)) are characterized by having a conduit structure through which the fluid drug formulation is delivered, by "poke and flow" approach [87,88]. These devices can deliver larger amounts of substances, when compared with the former types of MNs [89–91]. However, it is important to highlight that the clogging of needle openings with skin tissue during insertion raises some concerns [92]. To overcome this limitation, alternative designs suggest the bore-opening at the side of the needle [93]. Furthermore, the dense tissue around the needles causes flow resistance [94], which can be overcome by partial needle retraction after skin insertion [90]. A disadvantage of using hollow MNs is that liquid formulations require suitable and complex reservoirs [95].

Lastly, hydrogel-forming MNs (Figure 3 (e)) are prepared from cross-linked polymeric materials. The first systems were designed with a patch drug reservoir attached [96,97]. After insertion, the hydrogel needles take up ISF and swollen, allowing drugs from the back patch to diffuse through the structure into the skin. This device enables the intact removal of MNs array after use, leaving

no polymer residues behind. Another strategy involves the introduction of the drug formulation inside the array rather than in an external patch [98].

2.3. Manufacturing of MNs

MNs of a diversity of sizes and shapes can be fabricated using a plethora of methodologies (Figure 4) [43].

In the extensive body of information related to the preparation of MNs, the term microfabrication is usually reported. In fact, microfabrication refers to one precision field responsible to the development of small three-dimensional micron-sized structures by coupling serial direct-write technologies with precision machining methods [99]. The first MNs made of silicon were fabricated based on the conventional microfabrication technology, *i.e.* micro-electromechanical systems (MEMS) technology (Figure 4 (a)). It involves three basic techniques, namely deposition, patterning and etching [100,101].

The initial step consists in the deposition of thin films with varying thickness, from a few nm to about 100 μm. Then, patterning involves the transfer of a geometric pattern into the film. Lithography is used to transfer a pattern into a photosensitive material by selectively exposing it to a radiation source. Photolithography is the most commonly adopted process, but this step can also be performed using ion beam lithography, electron beam lithography, X-ray lithography and diamond patterning. The next phase involves etching (either wet or dry), which consists in cutting the unprotected parts of the material to generate the chosen design, either by using strong acid or mordant [21].

MEMS technology offers the advantage of allowing the fabrication of both solid and hollow MNs. However, this complex process involves multiple steps, requiring long fabrication time and clean room processing, becoming relatively expensive [101,102].

The fabrication of solid or hollow metal MNs can be performed by MEMS technology, electroplating or electrodeposition, photochemical etching and laser cutting [43]. The most simple method involves the manual assembly of conventional hypodermic needles [103]. Metallic MNs can also be integrated into a base substrate by magnetic assembly (Figure 4 (b)) [104]. As an alternative, to this technology, infrared laser can be used. In this case, infrared laser cuts the metal structures that are then bend at 90 °C, creating an out-of-plane array [105]. Besides laser cutting and manual assembly, metal MNs can also be produced using drawing lithography that allows the creation of relatively ultra-high-aspect-ratio metal MNs. It consists in using a thin layer of a thermosetting polymer which then follows controlled drawing by using pillars of defined patterns. This method enables the creation of three-dimensional solid long polymeric needles that can be employed as a mold to finally create hollow metallic MNs [106].

Glass MNs are prepared by pulling fire-polished glass pipettes using a micropipette puller. Then, the blunt-tip can be beveled at an angle of 35-38°. Usually, these MNs are attached to syringes [28]. On the other hand, ceramic MNs are generally fabricated using micromolding techniques, either by sintering processes or photo polymerization [43,107].

Micromolding is a set of fabrication methods which involves replicating microstructures using molds as master structures (Figure 4 (c)). It starts with the fabrication of the master MN templates, a structure containing a negative or inverse of the desired pattern geometry, followed by the preparation of the female molds. Then, the ceramic material is introduced onto female molds, followed by sintering or photo-cross-linking [108].

Polymeric MN arrays have been fabricated by using different manufacturing methods, namely micromolding techniques [56,109,110], which includes hot embossing [111], injection [99] and investment molding [112] and solvent casting [60]. Other processes include drawing lithography [113], electro-drawing [114,115], droplet-borne air blowing [113], photolithography [116,117] and continuous liquid interface production [118]. More recently, additive manufacturing by 3D printing has been studied [119,120]. These technologies take advantage of the versatility of this class of materials, in terms of viscosity, dissolution properties and post-modification. Micromolding is the most widely used method due to its cost efficiency, good reproducibility and scalability [108]. In this case, the polymeric material is introduced onto the female molds, and then the material is dried or photo-cross-linked, depending on the nature of the polymer. Finally, the MNs are peeled off from the female molds, which transcribe completely the microstructures of the master template. The use of master templates made of ceramics [98], poly(vinyl alcohol) [121], or poly(dimethylsiloxane) [63] has been reported. Among these, poly(dimethylsiloxane) has been chosen as the most interesting material for small-scale micromolding due to its good transcription ability, excellent thermo-stability, and poor adhesion, which is beneficial to the separation of the polymeric MNs arrays from the mold [122].

Some of the most common micromolding techniques are injection molding, hot embossing, and casting [108]. Injection molding requires the use of thermoplastic materials which are melted in the injection molding machine. Then, they are injected into the molds, where it cools and solidify into the final parts. The successful development of MNs depends upon a variety of factors, namely injection speed, mold cavity temperature, accuracy in design and manufacture of the master template [99]. In the hot embossing process, the mold and polymer are heated and pressed. Then, the mold is cooled to room temperature and the MNs arrays are demoulded [111,123,124]. By

polymer investment molding, two processes are combined, namely the traditional injection molding with investment casting, enabling the creation of hollow parts [112]. Another example involves the preparation of hollow MNs by casting, using a sacrificial templated produced through a double deep X-ray lithography process [111]. This fabrication process does not require a clean room environment and uses little instrumentation. Among the most common micromolding techniques, solvent casting is the most adopted [108]. Here, the polymeric material is placed into the female molds, followed by centrifugation or vacuum to fill the empty spaces and then drying or photo-cross-linking [98,125,126]. Despite the many advantages of micromolding, there are still some concerns for biomedical applications. First, the complex multiple fabrication steps are time consuming. Also, if heat or UV-light are involved in the fabrication process, the use of sensitive drugs, peptides, proteins and vaccines is rather limited [75].

To simplify the fabrication of MNs and preserve the biological activity of the active ingredients, a one-step fabrication procedure combining both shape-forming and solidification steps was reported. This technique, called centrifugal lithography (Figure 4 (d)), takes advantage of polymer solutions [127], and involves placing drops of polymer into a base (inner plate) of two parallel fixed plates, followed by centrifugation. The centrifugation step allows the drop to shape into an hour-glass structure, which will contact the outer-plate and solidifies the MNs. Finally, the plates are pulled in different directions, allowing the separation of two MNs from one-polymer drop.

A different strategy, the droplet air-blowing technique (Figure 4 (d)), uses forced air-blowing to shape the viscous polymer solution into MNs and involves six steps [113]. First, polymer droplets are dispersed over a flat substrate, used to support the MNs base. Then, in the second step, the drug droplet is dispensed over the baseplate and then, the upper plate follows a downward movement to enable contact with the dispensed droplets. On the fourth step, the upward movement of the

upper plate controls the length and then air-blowing is applied to solidify and shape the droplets. Finally, the two plates are separated to create two MN arrays on both upper and lower plates [113]. During fabrication, the thickness of the baseplate is determined by the volume of the polymer droplet dispensed in the first step. Drug loading can be easily controlled by the pressure and time of droplet dispensing. Compared to micromolding methods, the conditions of droplet-borne air blowing method are more moderate since neither heat nor UV irradiation is involved. The effect of two droplet-based fabrication methods, namely centrifugal lithography and droplet-born air blowing was compared, by analyzing the change in activity of the encapsulated drugs, namely epidermal growth factor which is known as an unstable peptide and ascorbic acid, an easily oxidized low-molecular-weight chemical compound. The results showed that centrifugal lithography exerts less stress during the fabrication, which involves low temperatures and vacuum-drying conditions, minimizing activity loss of the incorporated drugs. Furthermore, the morphological features and physical properties of the fabricated MNs, such as fracture force and morphology, were similar [61].

3D printing, also called additive manufacturing, was used as a method to fabricate MNs by adding materials layer-by-layer, by using a virtual Computer Aided Design model to create a physical object, in this case MNs [128]. 3D printing technology can use photopolymerization, in which UV-sensitive polymers are used and are layer-wise cured, allowing the construction of needles. 3D printers commonly used for printing thermoplastic materials include fused deposition modelling, as reported for the fabrication of poly(lactic acid) MNs [129]. It was also reported the 3D printing by stereolithography, as an example using a biocompatible resin [119,120].

Scaling up the manufacturing processes remains one of the biggest challenges of the pharmaceutical industry and process design is crucial to achieve standardization and cost-

effectiveness. The aforementioned technologies display several advantages and constraints. If, in the one hand, lithographic processes enable the preparation of highly complex shaped structures, the fact that is only applied to photo-curable polymers, time-consuming and involves a panoply of steps, can make it unattractive for industrial applications. On the other hand, centrifugal lithography or droplet air-blowing enable both shape forming and solidification at the same time under mild conditions, reducing the preparation time and technology needed. Nevertheless, post-processing might be required, and this approach only works with polymers within a certain viscosity range. Indeed, with the advent of 3D printing, which provides a high flexibility in the fabrication of complex structures, a more rapid development of these type of microstructures is expected in the near future. In brief, the successful translation of methodologies to manufacture MNs at an industrial level will depend on several factors, mainly on the nature of the material, stability of the active compounds, and the facilities required. In general, these core technologies have potential to ensure commercial-scale application, but their scale-up will always demand an adjustment and optimization of variables.

2.4. Mechanical properties

For MNs technology to become a reality, it is imperative to investigate the influence of a variety of factors related with their properties [130–132]. In general, the main factors affecting skin insertion ability of MNs are needle geometry such as shape, aspect ratio, and tip radius [132]. Since MNs experience a wide range of stress, particularly during insertion and removal, they must possess inherent strength to avoid failure, namely by bending, buckling and fracturing [133,134]. In this vein, mechanical evaluation of MNs is performed in order to infer about their efficiency and safety prior to use.

The first mechanical characterization of MN arrays was described by Zahn *et al*. [133], through the evaluation of the breaking strength of a single needle. In brief, this test consisted of a single, hollow silicon MN and a mechanical force gauge that gradually increased the vertical force applied at the tip (0-20 g) until it fractured. Since then, several tests have been employed to characterize the mechanical properties of MNs.

To infer about the mechanical properties of MNs, three tests can be performed, namely the axial and transverse fracture force tests and the three-point bending test (Figure 5).

The evaluation of the axial force involves applying a force perpendicular to the baseplate [82]. This test records both displacement and force while the MNs are pushed against a hard surface at a defined rate (Figure 5 (a)) [62,135]. When MNs fracture, a sudden decrease in the force *vs* displacement curve is observed. Needle failure force is determined by the maximum force detected immediately before this drop [135]. This test should be regarded with caution as some of the reports only use a single MN [132,133] and the failure force of a MN array cannot be strictly correlated with that of a single structure. Furthermore, this test does not fully simulate the forces experienced by the needles when inserted into the skin. Instead, they are compressed against a hard surface, which results in a concentration of the forces at the tip of the MNs, whereas during the penetration into a soft tissue the forces are distributed over a larger area [136].

The transverse fracture force test evaluates the behavior of MNs during insertion. Because of skin surface irregularities and its natural elasticity, the MNs arrays are not completely inserted and the transverse bending of the needles can be detected [62,135]. A mechanical test station is used and a force is applied to the MN *y*-axis at a defined point of the needle shaft (Figure 5 (b)). As aforementioned, a sudden drop in the force-displacement curve defines the MNs failure [62,82]. The main limitation of this test is the need to manually align the metal probe with a defined length

[82]. Even when this task is performed with the aid of a microscope camera, it still leads to experimental inaccuracies [62].

In addition to the mechanical testing of the MNs themselves, evaluating the baseplate is also important as the fracture of this component during patient application is not acceptable. Thus, this structure needs to be flexible enough to conform to the topography of the skin without fracturing. To evaluate the baseplate strength and flexibility, a three-points bending test has been used. The texture analyzer uses a metal probe to apply forces to the baseplates placed between two aluminium blocks. In this case, a maximum peak observed in the force-distance curve represents the force required to break the baseplate. The baseplate bending upon fracture is also determined to evaluate the flexibility of this structure [82].

Apart from the assessment of the mechanical properties of MNs, it is important to study the force required for MNs skin insertion. In this vein, Davis *et al.* [132] determined that about 0.08-0.34 N/needle were needed to ensure skin insertion of metal MNs in human volunteers. This data confirms the feasibility of manual insertion. Using hollow silicon MNs, the insertion forces were estimated to range between 0.10 N for the sharpest needle to 4.15 N for MNs with a blunt tip [137]. Furthermore, using ultra-sharp MNs, the insertion force can be reduced to below 10 mN [138]. On the other hand, Lhernould *et al*. [139] fabricated polymeric-based MNs using polycarbonate and confirmed that to ensure successful skin insertion, a maximum force of ~0.15 N/needle is required. Regarding MNs application, their success is determined by the ability to penetrate through skin. To evaluate skin penetration, transepidermal water loss measurements can be performed [140]. Microscopic techniques are also useful, either by application of a dye (Figure 6 (a)) over a skin surface [135] or by cross-sectioning and histological examination (Figure 6 (b)) [90].

Concerning the histological procedure, the preparation of samples might change the aspect of micropore structure. As a non-invasive methodology, optical coherence tomography (Figure 6 (c)) is useful, enabling the determination of pore diameter and depth [141]. The insertion studies are usually performed using biological tissues, either from humans or other animals like pigs or mice [142,143]. Notwithstanding the value of using biological materials, there are some constraints associated with the fact that the skin is usually heterogeneous, unstable, can be difficult to collect and its use must strictly comply with regulations for the use of human or animal tissues [144]. Therefore, Larrañeta *et al*. [145] reported the use of Parafilm® as a model membrane to simulate skin insertion. These authors folded the polymeric membrane into an eight-layer film to approximate skin thickness. Then, when comparing the insertion using neonatal porcine skin, the insertion depths were lower for Parafilm® but proved to be useful as an alternative to biological tissue for MNs insertion studies.

In sum, to ascertain the mechanical properties of MNs, a variety of tests can be performed. At the same time, the diversity of needle geometry and size coupled with the assortment of tests makes the comparison between MNs quite difficult. In this case, MNs technology and development would benefit from standardization of procedures to evaluate their mechanical performance.

3. Biopolymer-based microneedles

A wide range of polymers derived from biological systems, *i.e.* biopolymers, has been employed in the fabrication of MNs. Biopolymers, such as polysaccharides (*e.g*., hyaluronic acid (HA) [146,147], CS [40], cellulose [67,148]), proteins (*e.g*., gelatin [39,69], silk [149–151] and collagen [148]) and DNA [152], have been used directly in their native form or after chemical modification

(*e.g.*, methacrylated hyaluronic acid [38], carboxymethyl cellulose [153–155]), alone, as blends or composites.

Polysaccharides and proteins play a paramount role in the development of MNs and therefore are the focus of this review article. These two classes of biopolymers share some chemical similarities with the components of extracellular matrix and are easily recognized and accepted by the human body [156]. After absorption, they follow elimination by metabolism or excretion through the renal system, considering that they are below the glomerular threshold, avoiding tissue accumulation [157]. In this sense, polysaccharides and proteins used in MNs development are either approved by the FDA (US Food and Drug Administration) or classified as GRAS (generally recognized as safe) [158,159].

Polysaccharides and proteins exhibit a great structural diversity and many inherent properties, which influence the mechanical properties and penetration ability of MNs and determine the bioactivity and stability of the pharmaceutical ingredients [160–162]. Specific properties such as polymer weight, swelling behavior, and possible interactions between the biopolymer and the drug will influence and tailor drug release rate [3,157,163]. Naturally, these myriad features influence their *in vivo* dissolution behavior and polysaccharide and protein-based MNs can be grouped into dissolvable, biodegradable and swellable devices, as summarized in Table 1 and discussed in the following paragraphs.

Dissolvable biopolymeric MNs are fabricated using water-soluble macromolecules which dissolve after skin insertion [35], namely using dextran [162,164], sodium chondroitin sulphate [143,162], HA [85], gelatin [155], a collagen-enriched extract from fish scales [148,165,166] or dissolved silk fibroin [167]. In general, the array dissolves within several seconds or minutes upon skin insertion. The fast dissolution is accompanied by the quick release of the pharmaceutical agents,

which makes them suitable for instant drug release [160–162]. Incorporating different molecular weights of the same polymer or other components can tailor the dissolution profile. Hence, dissolution matrices amenable for prolonged DD can also be fabricated [168]. Dissolvable MNs are poised to provide a beneficial route to the administration of biopharmaceuticals in the lower-microgram range, in smaller doses than those administered using injections, reducing not only the systemic effects but also the treatment costs [169]. Additionally, because the drug formulation is incorporated as part of the dissolving matrix, drug loading and release is precise. However, the lower mechanical strength of dissolvable MNs may difficult skin insertion.

Biodegradable MNs are fabricated using polysaccharides and proteins that degrade after skin insertion [149,170]. The term biodegradation refers to the degradation process that takes place in a biological environment, in this case, inside the body under the influence of enzymes [171]. Usually, mechanisms of biodegradation may require a gradual breakdown of the material which is a longer process when compared with dissolvable MNs. Therefore, biodegradable MNs are very attractive for sustained DD. One of the major features that convey significant impact on the capacity of these biopolymers to be used in biomedical devices is their relative degradation rate, that can be modulated to provide flexibility in drug release [149,170].

Non-water soluble polysaccharides and proteins such as chitin [172], CS [173,174], starch [175] and silk [7,63,149,172,173,176] are the most used. More recently, suckerins, proteins extracted from squids, were also studied in the fabrication of biodegradable MNs [71]. Regarding the biodegradation ability of MNs, Yin *et al*. [151] evaluated the enzymatic degradation of modified silk MNs *in vitro*. To mimic the ISF, collagenase I and protease XIV were added to in PBS (phosphate buffered saline). After incubation using protease XIV for 10 days, silk MNs modified using 2-ethoxyethanol displayed more than 65% mass loss.

Regarding swellable polysaccharide and protein MNs, these are fabricated using hydrogels which due to their cross-linked structure, swell in the skin without dissolving [38,151]. On behalf of this feature, these biopolymers allow not only the release of preloaded drugs but also the extraction of ISF [177]. To create swellable MNs it is reported the use of methacrylated HA [38] and modified silk [151]. Compared to the aforementioned types of MNs, these deposit no tip materials in the skin and have flexibility to stop the treatment if adverse drug reactions or overdose occur [178]. Typically, the swelling ability of these biopolymers is controlled by their cross-linking degree, which in turn tailor the drug release rate [179]. It is important to highlight that these MNs should have sufficient mechanical strength in the dry state to allow penetration into the *SC* and partially retain this toughness in the hydrated state, in order to enable the intact removal from the skin.

According to their performance *in vivo*, polysaccharide and protein MNs are employed in the transdermal drug delivery of small molecules, nanomedicines (*e.g.* nanocapsules) and biotherapeutics (*e.g.*, proteins, peptides or vaccines). Polysaccharide and protein-based MNs are designed to meet the properties of their cargos enabling DD through bolus or sustained administration. The pharmaceutical ingredients can be incorporated into the MN matrix, namely the tips, base or backing adhesive layer, or coated onto the surface of the structure. To control drug release, drugs can also be preloaded into nanoparticles which are then encapsulated in the matrix [17,18,42,180]. Besides drug administration, biopolymeric MNs have also been studied in fluid extraction for diagnosis and lastly, for cosmetic purposes [18]. The next sections will give an overview of the applications of polysaccharide and protein-based MNs and explore their usefulness and challenges for potential clinical application.

3.1. Polysaccharides-based MNs

The recent trend of using polysaccharides in the preparation of biomaterials has naturally been extended to the fabrication of MNs [181]. In fact, polysaccharides like HA [182–185], CS [186–188], and dextran [189], among others [67,190], have been used alone or combined with other biopolymers such as amylopectin [153,154,160,168,191] to engineer MNs for the delivery of drugs such as doxorubicin [192] and lidocaine [193], biopharmaceuticals such as insulin [175,194,195] or vaccines [196], and also natural extracts. The next sections give an overview of polysaccharides used in MNs. Table 2 highlights some of the most recent examples of polysaccharide-based MNs reported in literature in terms of basic components, pharmaceutical ingredients and outcomes of their application.

3.1.1. Hyaluronic acid MNs

HA is a major component of the extracellular matrix and cartilage with mucoadhesive properties [3]. This polysaccharide has negative charge and the salt form is highly soluble in water. In this vein, HA is mainly used in the fabrication of dissolvable MNs, as reported by Matsuo *et al*. [183]. Using MNs of 200, 300 and 800 μm in height these authors found that after insertion into mice and rats skin, the needle tips dissolved within 5 min and the body structure fully dissolved in 1 h (Figure 7) [182]. Kang *et al*, [147] fabricated adenosine-loaded HA MNs for cosmetic purposes and found that 15 min after insertion into porcine skin the needles were fully dissolved, with a penetration depth of 92% the needle height. During a 10-week clinical test, the use of HA MNs improved skin wrinkling, density, elasticity and hydration when compared with the topical cream application.

Instead of incorporating the pharmaceutical ingredients into all the needle matrix, Liu *et al*. [146] studied the fabrication of tip-loaded HA MNs which dissolved within 30 seconds. In this work,

the transdermal delivery of exendin-4, a glucagon-like protein-1 receptor agonist, which mimics the activity of mammalian hormone glucagon-like peptide 1, was studied and fluorescein isothiocyanate (FITC) labelled dextran was used for the permeability tests. *In vitro* studies showed an initial burst release during the first 30 sec and most labelled dextran was dissolved within 5 min. When comparing with subcutaneous injection of exendin-4 in type 2 diabetic rats, the MNs produced similar plasma concentration profiles and had comparable effects on glucose tolerance and insulin secretion, indicating that exendin-4 loaded HA MNs can be used as an alternative for treatment of type 2 diabetes.

On a different perspective, Chen *et al.* [197] fabricated HA MNs that dissolved within 10-15 min. These needles were designed with a deep cave to pack directly live attenuated Bacille *Calmette–Guerin* bacillus (Figure 8 (a)), the only licensed vaccine for tuberculosis prevention. With this strategy, the vaccine powder was exposed to skin ISF (Figure 8 (b-c)), dissolved and diffused into skin. After 6 h it was spread into the epidermis and after 19 h most vaccine had diffused through skin (Figure 8 (d)). Overall, this study confirmed the successful delivery without inducing over inflammation.

Additionally, vaccine's viability and the penetration ability of MNs was almost not altered during 60 days of storage at room temperature [197]. Accordingly to the World Health Organization (WHO), Bacille *Calmette–Guerin* vaccine is stable for at least two years when stored at 2-8 °C [198].

Despite the short-time stability of Bacille *Calmette–Guerin* into MNs, when compared with the conventional method, this study shows the usefulness of these devices in non-developed areas where cold chain storage is not possible, and the fast administration is the purpose. The authors,

opened new perspectives in this area of vaccine technology, showing that MNs are also useful for vaccine storage, with a universal methodology that simplifies fabrication and preparation [197].

Regarding the delivery of nanomedicines, Wang *et al*. [85] fabricated HA MNs with pH-sensitive dextran nanoparticles incorporating anti-PD-1 (aPD1, antibodies that block the programmed death-1 pathway) and glucose oxidase (Figure 9).

The MN matrix was fabricated using cross-linked HA by *in situ* photopolymerization of *N,N′*-methylenebis(acrylamide). The nanoparticles are composed of an acid-degradable polymeric matrix, fabricated by derived dextran (conjugated with ethoxypropene enabling substitution of hydroxyl to acetal group), alginate (a polyelectrolyte surfactant), glucose oxidase/catalase system and aPD1.

Hence, this system was applied towards a melanoma site with a simple administration. Dextran nanoparticles convert glucose into gluconic acid, creating an acidic environment which then promotes nanoparticle dissociation and release of the antibodies (Figure 9 (a)). These authors found that a single administration induces robust immune responses in B16F10 mouse melanoma (Figure 9 (b)). The release of aPD1 was pH-dependent and glucose-mediated and the bioactivity of the antibodies remained at over 90% after one-month storage at 4 °C. This system did not induce any significant decrease in cell viability and skin recovered quickly, with no significant inflammation detected 2 days after administration. This work allows concluding that the antitumor ability of the MN patch is due to the sustained release of aPD1 and the enhanced retention in a tumor microenvironment.

Despite these biomacromolecules, the incorporation of cells was also studied. For instance, HA MNs loaded with adipose-derived stromal vascular fraction cells was evaluated on diabetic wound healing. Cell incorporation resulted into an accelerated wound healing in porcine models when

compared with HA MNs or the use of cells fraction alone. Therefore, the local administration of HA and derived cells using MNs may be an alternative method for treatment of wounds in diabetic patients [199].

In a different perspective, to decrease the dissolution rate and increase the mechanical strength of HA microneedles, Park *et al*. [168] introduced amylopectin into a MNs system designed to deliver model cosmetic ingredients, namely niacin and ascorbic acid. In this study, the mechanical strength of the MNs increased with increasing amounts of amylopectin added up to a ratio of 1:2.3 (HA:amylopectin). However, higher amylopectin contents led to stiffer and brittle structures, too difficult to peel off the mold without breaking. Dong *et al*. [200] fabricated HA MNs loaded with Au nanocages and doxorubicin. These Au nanoparticles were incorporated to reinforce the mechanical properties of the dissolving MNs and to make use of their excellent photothermal effect. Hence, this system initiates a photothermal effect after irradiation using near-infrared light, which coupled with the chemotherapeutic effect of doxorubicin, is able to synergistically destroy superficial skin tumors.

In a different perspective, to tailor drug release, Kim *et al.* [201] added trehalose and poly(vinylpyrrolidone) to HA MNs and found that both additives could facilitate the release of peptides. It was also found that poly(vinylpyrrolidone) may prevent peptide aggregation and enzymatic degradation, resulting in a more efficient diffusion of the drug into the systemic circulation.

Besides the incorporation of other polymers or particles, the functionalization ability of biopolymers is evidenced by a study reported by Wang *et al.* [18] In literature, the development of swellable MNs using methacrylated HA for timely metabolic analysis (Figure 10 (a)) is reported [85].

This chemically modified biopolymer was prepared by reaction of HA with methacrylic anhydride followed by cross-linking of the methacrylated moieties by radical polymerization under UV light at different times, from 3, 5, 10 to 15 min. Methacrylated HA MNs showed full skin insertion after being pressed with 1.5 N into porcine skin. The patch was removed intact from skin and only a slight deformation of MNs was detected, as a result of swelling. The swelling speed of these MNs is similar (Figure 10 (b)). They swell visibly within the first 5 sec and reach a plateau within 1 min, regardless of the previous UV exposure time. Nevertheless, the swelling ratio provided different results and the lower the cross-linking degree, less liquid is extracted by the patch. For example, MNs prepared with 3 and 15 min of UV exposure were able to extract liquid as nine and two times its own mass, respectively as a reflex of the increasing network density. In addition, a lower network density is related with an easy recovery of the extracted fluids from the MNs. After insertion into mouse skin *in vivo*, the patches were able to extract 1.4 mg of ISF after 1 min and about 2.3 mg after 10 min. Furthermore, 30 min after removal, the skin spots were recovered indicating decreased potential of infection. Still, despite deformation by liquid absorption, all MN arrays were able to retain shape and left no residual waste in the skin. Hence, this study was an important contribution to demonstrate the possibility of ISF extraction using MNs since this fluid makes up to 45% of the volume fraction of human skin (Figure 10 (c) and (d)).

Cross-linking HA using 1,4-butanediol diglycidyl ether tailors the degradation and swelling ability of HA MNs, enabling tailoring drug release [64,65]. MNs formulated with cross-linked HA are proposed to delay drug release. HA solutions are highly viscous solutions and MNs display no permanent swelling behavior is due to its water-soluble character whereas cross-linked HA forms an hydrogel in water that lasts longer after swelling due to retarded enzymatic degradation [64].

Zhang *et al*. [65] formulated HA MNs with HA particles cross-linked using 1,4-butanediol diglycidyl ether. The incorporation of HA particles improved the MNs mechanical strength and decreased the degradation of the matrix by enhancing the *in situ* swelling ability.

Therefore, these MNs are more interesting for prolonged drug delivery of HA, used as dermal filler for cosmetic anti-wrinkle treatments. Another cross-linking methodology was described by Larrañeta *et al*. [202] who prepared hydrogels using HA and Gantrez S97, a copolymer of methyl vinyl ether and maleic acid. The multiple acid groups of Gantrez, enable the establishment of ester bonds with HA hydroxyl groups. Hence, using methylene blue as a model molecule, these authors found that HA cross-linked MNs can sustain the release up to 2 days. Due to the antimicrobial ability of these hydrogels, these MNs are proposed to mitigate device-associated infections.

Monkärë *et al*. [169] fabricated IgG-loaded HA MNs, avoiding elevated temperatures or high pH. As a result, they found that about 82% of the protein was recovered and fluorescence microscopy unveiled that its tertiary structure was not changed after MNs fabrication. Liu *et al.* [184] found that storage of insulin-loaded HA MNs at −40, 4, 20, and 40 °C during a month did not altered the stability of the peptide, with more than 90% of insulin detected in the MN patches. Furthermore, the authors also found that insulin is rapidly released from MNs after storage. The complete dissolution and delivery of insulin-loaded MNs within 1 h and that MNs containing from 0.13-0.44 U of insulin promoted a decrease in glycemia levels from 43% to 88%, tuning the hypoglycemic response were demonstrated. In a different study, HA MNs incorporating *all-trans* retinoic acid (used as model compound due to its poor water solubility), dissolved almost completely in 2 h, delivering up to 90% of its content. During the first hour, only 76% of the *all-trans* retinoic acid was delivered and the structure was not completely dissolved. Then, to establish the stability of *all-trans* retinoic acid and tetanus toxoid/diphtheria toxoid divalent vaccine into

HA MNs they were stored at different temperatures. Retinoic acid content was reduced to 78% after 1 week at room temperature (25 °C) and after 24 weeks the reduction reached 45%. On the other hand, during 24 weeks under refrigerated conditions (4 °C) a decrease of 13% was observed. Regarding the tetanus toxoid/diphtheria toxoid vaccine, the MN arrays were stored during 6 and 12 months at 4, 25 and 40 °C in heat-sealed aluminium laminated sachets. After vaccination of rats, both anti-tetanus toxoid and anti-diphtheria toxoid titers were induced, showing that storage temperature did not affected the loaded tetanus toxoid and diphtheria toxoid and hence, the immune response [182].

In addition, HA MNs inhibited ascorbic acid 2-glucoside degradation after e-beam sterilization (40 kGy). HA MNs maintained their morphological features and fracture force after sterilization and did not affect the dissolution rate and drug release of HA MNs. Furthermore, sterilization could effectively reduce microorganism and endotoxin contamination levels. This work shows the potential in using HA as a biopolymeric matrix which offers the advantage of allowing the sterilization requirements without activity loss of encapsulated pharmaceuticals [201].

3.1.2. Chondroitin sulphate MNs

Sodium chondroitin sulphate is used inexhaustibly in the fabrication of biomaterials, and similarly to HA, is a component of the extracellular matrix and cartilage [3] and the salt is highly soluble in water [66]. Fukushima *et al*. [66] studied the transdermal delivery of human growth hormone and desmopressin in rats using MNs fabricated with sodium chondroitin sulphate and dextran. In this study, the MNs performed similarly and the pharmacokinetic profile was characterized by a fast attainment of peak concentration at the first 15 min. Then, it was followed by a gradual decrease in human growth hormone plasma levels, with a terminal half-life of around 25 min. Upon

application of both sodium chondroitin sulphate and dextran-MNs, these authors found a direct relationship between dose and concentration. Furthermore, drug bioavailability was about 95% in sodium chondroitin sulphate MNs and 73% in dextran MNs. When compared with the intravenous injection, human growth hormone displayed much shorter elimination half-life, of about 4 mins. Therefore, the increased terminal half-life of 25 mins upon MNs application is attributed to the absorption rather than to the elimination phase. Regarding desmopressin (1.07 kDa) delivery, sodium chondroitin sulphate needles showed an absorption phase half-life of 14 mins and the pharmacokinetic profiles were characterized by a peak concentration within the first 30 min. Also, a terminal half-life of approximately 2 h was determined. Regarding storage, these devices proved to be stable for at least 1 month under refrigeration or freezing conditions. Yukako *et al*. [40] studied the administration of leuprolide acetate, with 1.2 kDa) using sodium chondroitin sulphate MNs and reported a low bioavailability of the peptide. In vitro tests showed that the peptide was released within 3 min. Then, after application into rat skin, plasma concentration reached its maximum within 15 min whereas 20 min were necessary for sodium chondroitin sulphate administration. Nevertheless, the degradation rate of leuprolide acetate was very fast leading to only 32% of drug being bioavailable.

3.1.3. Cellulose based MNs

Carboxymethyl cellulose and (hydroxypropyl)methyl cellulose are cellulose derivatives widely used for biomedical purposes. These water-soluble polymers are mainly employed due to their ability as thickening, binding and stabilizing agents, and also due to their film-forming ability [203,204].

Kim *et al.* [205] reported the development of (hydroxypropyl)methyl cellulose MNs incorporating donepezil hydrochloride (an acetylcholinesterase inhibitor used in the treatment of Alzheimer's disease) in the needle tips. In this work, over 95% of the drug was delivered within 5 min of insertion and all MNs were fully dissolved in skin within 15 min.

Zaric *et al*. [206] prepared MNs using carboxymethyl cellulose and used sucrose as protein stabilizer. A recombinant human adenovirus type 5 vector encoding HIV-1 gag, to generate robust antigen-specific $CD8^+$ T cells in the tissue was also added. The MN patch was able to dissolve about two-thirds in length within 3 min of application, which was appropriate for effective delivery of the virus onto the dorsal skin of mice. In this study it was shown that this type of vaccination leads to the production of antigen-specific $CD8^+$ T cells, validating the delivery efficiency of the MN patch. In this case, the major problem in vaccine administration using MNs is overcome, since it is possible to maintain the immunogenicity of live vaccines after lyophilization or drying. These are retained at the mucosal sites and can quickly expand in response to locally released antigenic challenge. If these advantages are combined with the benefits of using MNs, namely easy storage and transportation, with no cold-chain requirements, increased safety as no sharp wastes generated, easy self-administration and patient compliance, these MNs can easily be translated into clinic applications. Using carboxymethyl cellulose MNs, the administration of probiotics was also evaluated using *Lactobacillus*. The effectiveness was supported by the production of lactic acid *ex vivo* in pig skin and *in vivo* in rats. This work demonstrates that the probiotics delivered by MNs were bioactive and functional in a pain-free manner and may improve local skin health and immune functions [207]. In a total different vein, Lahiji *et al*. [208] reported the fabrication of carboxymethyl cellulose MNs incorporating valproic acid to induce hair regrowth (Figure 11 (a)).

After incorporation into MNs, the active ingredient showed no activity loss, proving to activate Wnt receptor cells, which are involved in initiating hair follicle growth. The cumulative release of valproic acid using MNs was higher and faster than using a topical formulation. About 120 min after application, 87% and 21 % of valproic acid was delivered using MNs and topical formulation respectively, showing the higher efficiency of valproic acid delivery using MNs. Finally, to evaluate hair- regrowth, valproic acid was administered into mice skin at telogen phase, once a day, for 28 days. The results showed that at the last day of treatment, mice treated with valproic acid-loaded MNs and two (out of seven) treated with topical valproic acid evidenced hair regrowth (Figure 11 (b)). Using topical valproic acid, the hair regrowth mostly in the center of the shaved area, whereas the use of MNs led to a uniformly covered area, with high accuracy over the affected area. Consequently, more hair follicles were found on skin of valproic acid-loaded MNs (Figure 11 (c)). Overall, valproic acid-loaded MNs elevates hair follicles regrowth, accelerating telogen-to anagen transition, with clear evidence of not damaging the hair shafts or the epidermis layer.

3.1.4. Chitin and chitosan MNs

Chitin is the second most abundant natural polysaccharide, after cellulose, and by deacetylation originates CS, a polysaccharide widely studied for biomedical applications [172–174]. At slightly acidic aqueous conditions, CS possesses a high density of positive charges which enables tissue adhesion and mucoadhesion [209]. CS is degraded by hydrolysis of the acetylated residues and its degradation rate is correlated with the molecular mass and its deacetylation degree [157]. The conversion to glucosamine derivatives, which are excreted or used in the amino sugar pool, avoids CS accumulation in tissues [210]. In addition, FDA recognizes CS as GRAS and is approved for use in wound dressings and cartilage repair [159,211,212]. Furthermore, some CS-based

formulations for drug delivery are being studied in clinical trials [212]. Chitin and CS have also been used for the preparation of MNs for sustained drug delivery. Jin *et al.* [172] prepared biodegradable coated chitin MNs arrays, for tuberculosis skin test. Chitin MNs are mechanically robust and physiologically inert, water-insoluble and did not showed significant swelling. Upon application to guinea pig skin, these MNs ensured the delivery of a mixture of tuberculosis antigens that gave a true- positive test, confirming the potential of using these MNs as a convenient diagnostic tool [172].

Chen *et al.* [173] fabricated biodegradable CS MNs for sustained delivery of bovine serum albumin (BSA). Using a homemade applicator these CS MNs were easily inserted into porcine skin and after 30 min a burst release of 20% BSA was detected. Then, in the following 8 days, a slower and sustained release was observed, with 95% of BSA released during this time. However, this study showed that CS MNs soften and break after insertion, leaving behind some polymeric parts that were detected in skin, in the 4 days after insertion. Regarding proteins stability, circular dichroism revealed that both the fabrication procedure and storage were gentle enough to avoid denaturation of the model protein, which unveils the usefulness of using CS MNs to incorporate a myriad of biopharmaceuticals [173]. In a distinct study, Chen *et al.* [188] reported the fabrication of CS MNs to allow a sustained release of the model antigen ovalbumin (Figure 12 (a)).

This implantable system comprises a dissolving backing layer of a synthetic polymer, poly(L-lactide-co-*D,L*-lactide), to overcome skin indentation during insertion and provide a more effective skin penetration. The needle tips are composed by ovalbumin-loaded CS. After insertion, the back-layer dissolves and the CS tips release ovalbumin (Figure 12 (b)). The micropores produced due to skin disruption were not detected after 6 h. Histological section of rat skin showed that the implanted MN tips became smaller with time and at the 28th day, there was still fluorescence of

the Alexa-ovalbumin in the small MN tips. Considering the biodegradability of CS within 3-4 weeks, this study suggests that these devices can release antigens within a timeline of 4 weeks (Figure 12 (c)). Regarding the *in vivo* release behavior, about 50% of the antigen was released from the MNs within the first two days and after 3 weeks little fluorescence was detected (Figure 12 (d)).

In addition, CS MNs enabled immunization with a lower dose of antigen, decreased from 500 to 200 µg, a 2.5-fold reduction, when compared with conventional injection. These MNs induced a stronger immune response probably by prolonging antigen retention in skin. Overall, this system offers the benefit of guaranteeing the delivery of the intended dose into skin avoiding waste, providing useful option for long-term delivery of vaccines into skin. Interestingly, this study demonstrated immunization with one administration of non-living antigen, which is usually difficult with a single injection, as it usually fails to elicit robust and durable immunity.

By using the same system, in which CS needles are the tips of a dissolvable system, Chen *et al.* [186] delivered luteinizing hormone analogs, currently the androgen-deprivation therapy used in the management of prostate cancer. After MNs application in mice, these authors detected an increase in serum luteinizing hormone levels which declined at day 7. Testosterone increased up to day 14 and then declined to at day 21, producing a castration state and proving the usefulness of these CS MNs into an androgen-deprivation state.

3.1.5. Starch-based MNs

Starch is a natural polysaccharide with a long tradition in the pharmaceutical industry [213]. Its ease of processing and filmogenic ability when gelatinized, make it attractive for the development of materials for biomedical applications [214]. In the development of MNs, it was blended with

other biopolymers due to its brittle behavior. Ling *et al.* [175] physically blended starch with gelatin to deliver insulin and found that MNs penetrated to approximately 200-250 μm, about one third of the needle length. In addition, they delivered the entire payload in the first 5 minutes and efficiently lowered blood glucose levels. Interestingly, it was found that more than 90% of the insulin was stable after storage 25 or 37 °C for one month. This indicates the convenience of using these starch MNs while reducing the cost of cold chain storage and transportation.

3.2. Proteins-based MNs

Regarding protein-based MNs, these have been fabricated mainly with gelatin [69,195,215] and silk [63,150,151,176] for the delivery of small drugs, namely lidocaine [148] and tamoxifen [70], and biopharmaceuticals, namely insulin [39,195] and vaccines against influenza, *Clostridium difficile*, and *Shigella* [176]. Other proteins from animal source, particularly suckerins [71] and collagen extracts [166], are seldomly employed. A general overview of the proteins used in the fabrication of MNs is given in Table 3.

3.2.1. Gelatin MNs

Gelatin is a water-soluble biopolymer which results from the partial hydrolysis of collagen from skin. Due to its highly conserved domains, gelatin promotes cell adhesion with a non-immunogenic response, with relevance for biomedical purposes [216]. Regarding the fabrication of gelatin MNs, An *et al*. [69] reported its use as the structural material and the component for biological activity. The intracutaneous delivery of gelatin proved to locally reduce the adipose tissue (Figure 13). MNs were inserted into skin for 2 days (Figure 13 (a)) and Franz diffusion tests showed that 70% of the dissolving polymer diffused through the skin layer. *In vivo* tests using rats showed that after

application of gelatin MNs the adipose tissue weight was reduced by 20% when compared with the control. In addition, the fat area was reduced by 60%, with clear evidence of adipocyte size reduction with subsequent shriveling. In particular, gelatin administration is correlated with repressed transcription of lipogenic enzymes and an ability to reduce fat accumulation. Overall, this biopolymer was used not only as structural element but also as the active agent which can regulate fat metabolism and have an active role in local reduction of fatty tissue. These MNs open new perspectives regarding the incorporation of other pharmaceutical ingredients such as anti-obesity active principles.

Gelatin and sucrose based MNs were studied for the delivery of inactivated polio vaccine [217]. Gelatin MNs were able to penetrate pig and monkey skin and dissolved almost completely after 15 minutes leaving no residual sharp wastes (Figure 13 (a)).

Inactivated polio vaccine administration showed that after the first week the neutralizing titers were weak. However, 100% seroconversion was achieved as reflected by the dramatically increase in the antibody titers (Figure 13 (b)). Therefore, using gelatin MNs for polio vaccination displayed immunogenic ability in rhesus macaques and may offer a simpler method for mass vaccination to facilitate polio eradication.

As water dissolving matrices, gelatin MNs dissolve quickly and different strategies have been studied aiming to control drug release. Yu *et al*. [68] prepared bio-ceramic MNs by adding hydroxyapatite to gelatin in the formulation of the DD devices. These MNs exhibited low cytotoxicity against RAW 246.7 cells and excellent cytocompatibility for maintaining biological activity of insulin. In the administration of insulin using MNs the results showed that insulin concentration increases quickly and then declines slowly. On the other hand, the subcutaneous injection of insulin leads to a sharp increase of the plasma insulin concentration and then decreased.

Hence, and owing to the fact that plasma insulin level can be maintained for longer periods of time, insulin delivery is sustained.

Using genipin as cross-linking agent in rapidly separating gelatin MNs, Chen *et al*. [218] found that insulin delivery could be tailored (Figure 14).

The incorporation of PVA as a back layer allows the proper insertion and dissolution of gelatin tips into skin (Figure 14 (a-b)). The degree of cross-linking enhances the mechanical strength and the resistance to humidity. Furthermore, the *in vitro* (Figure 14 (c-d)) and *in vivo* insulin release tests showed significant changes in the release rates in MNs with different cross-linking degrees. The hypoglycemic effect in diabetic mice demonstrated that the higher cross-linking resulted in controlled insulin release compared with other treatments and prolonged effectiveness in virtue of genipin as a cross-linking agent for producing biocompatible MNs.

3.2.2. Silk fibroin MNs

Silk consists mainly of two proteins, *i.e*., silk fibroin which constitute the center of silk and sericin, hydrophilic proteins that coat these fibers. Silk fibroin is a protein approved by FDA for biomedical purposes, insoluble in water and characterized by β-sheet structure with high tensile strength and toughness [219]. Silk degradation occurs due to the action of proteolytic enzymes such as chymotrypsin, actinase and carboxylase. First, the protein is adsorbed by different enzymes through binding domains on the protein's surface. Then, after digestion, the amino acids are easily absorbed [220,221]. The interest in using dissolved silk fibroin, relies on the fact that this protein generates non-inflammatory products, which can be metabolized by cells [221]. In addition, this matrix possesses adjustable mechanical properties owing to its crystalline domains responsible for improving rigidity and therefore, the mechanical strength of MNs [167].

Regarding the preparation of MNs from silk fibroin, Raja *et al*. [7] studied the fabrication of a series of arrays with various shapes and sizes. Different strategies of drug loading demonstrated the ability of using silk fibroin to tailor DD. Loading BSA directly in the MN array enabled a sustained delivery of the compound, with only 0.4% being released after 16h of insertion. The maximum drug released was achieved using MNs loaded and coated with drug leading to more than 5 μg of BSA delivered in 3 h. After 16 h, almost 10 μg of drug was delivered from the MNs loaded and coated with drug. This study unveils the successful use of silk fibroin in tuning drug release and can be useful in providing a sustained administration of macromolecules.

On the other hand, Stinson *et al*. [176] reported the fabrication of silk fibroin MNs for vaccination purposes. These needles were coated with *influenza*, *Clostridium difficile*, and *Shigella* vaccine antigens, and silk fibroin to provide thermostability during drying and storage. After application into mice skin, humoral responses were generated confirming the successful delivery of antigens. Owing to the incomplete elution of the antigens from the patch, the specific IgG and IgA were lower than those obtained after injection with the same dose. However, these results are promising and the preparation of silk fibroin MNs offer good potential in the MNs area.

Yin *et al*. [151] reported the fabrication of a swellable MN system based on modified silk fibroin. Herein, the authors prepared swellable MNs by blending silk with different low molecular agents (urea, glycine, dimethylformamide and 2-ethoxyethanol). The modified resulting silk fibroin MNs exhibited decreased dissolution abilities and an extraordinary swelling property. The 2-ethoxyethanol-silk fibroin MNs were the most promising ones, showing minimal dissolution, less than 10%, and a great swelling ability (500%) at a mixing ratio of 1:10 (w/w). These MNs successfully penetrated skin and after introduction into PBS it is possible to verify that there is a correlation between pore dimension and swelling ability. For instance, a swelling ratio of 650%

can be achieved using a ratio of 0.5:10 (2-ethoxyethanol:silk fibroin) and using a ratio of 3.0:10, a swelling ratio of 250% can be achieved. To access the enzymatic degradation *in vivo* these authors used protease XIV and collagenase I and found that there is a negative correlation between degradation and blending ratio. For instance, MNs fabricated with 0.5:10 (2-ethoxyethanol:silk fibroin) exhibited more than 65% mass loss within 10 days using protease XIV. This assay also shows that these swellable systems do not cause irritation or skin sensitization. Using these swellable silk MNs, the release of FITC-dextrans was about 2-10 times larger than the corresponding control. In this process of drug administration, the porous dimensions play a critical role. Also, the release profile unveils that there is a direct relationship between releasing kinetics and swelling ability. Higher swelling MNs incorporating 40 kDa FITC-dextran exhibited higher releasing kinetics than MNs with lower swelling degrees (250%) and incorporating 20 kDa FITC-dextran. Therefore, this type of system holds a huge potential in controlled delivery systems.

On a different perspective, DeMuth *et al*. [222] fabricated silk MNs for enhanced immunogenicity by loading vaccine into the silk tips. These silk tips were implanted into a MN system with a dissolvable base. After dissolution the silk material remained in skin releasing the immunogenic agent, for two weeks. MNs loaded with a fraction of vaccine dose induced stronger $CD8^+$T cell proliferation, increasing percent $tetramer^+$ $CD8^+$ T cell proliferation. Furthermore, silk loaded tips led to increased induced 10-fold higher T-cell and humoral responses when compared with injection.

3.2.3. Other protein-based MNs

Suckerins, are a group of proteins extracted from jumbo squid and characterized by containing a high content of β-sheets as building blocks which in turn, self-assemble into a supramolecular

network. These proteins are reported to be useful due to their thermoplastic properties and solubility in weak acidic solvents [126,223,224]. Ding *et al*. [71] prepared MNs based on suckerins with good penetration ability (Figure 15 (a)).

Their mechanical strength can be tuned by a variation of pH or by the addition of a hydrogen bond disruptor, which tailor the secondary structure of these proteins and hence, their drug release ability (Figure 15 (b)) These authors were able to tailor the Young's modulus of suckerins-based MNs over nearly 6 orders of magnitude simply by incubation in different pH solutions or urea. This data suggests a direct relationship between Young's modulus and β-sheet content which is consistent with the load bearing functionality of nanoscale β-sheets. The authors took advantage of exploiting the easy of processing, biocompatibility and β-sheet induced supramolecular self-assembly. A decrease in elastic modulus in MNs is associated with increased swelling and hence, chain mobility, inducing an increase in the mesh size of the polymeric network, which is then expected to increase the permeability for drug diffusion [71]. Using rhodamine, a fast drug release was observed in the first 10 h and after that a continuous sustained release was observed over time. With 2 M urea, up to 28% rhodamine was released after 100 h (Figure 15 (c)). After the incorporation of an antibiotic agent, kanamycin, a decrease in bacterial density was detected after MNs insertion (Figure 15 (d)). Regarding the biocompatibility, human dermal fibroblasts were selected for this study and upon contact they started to spread and continued to proliferate up to day 7 with almost no dead cells observed.

Fish scale biopolymer, a collagen enriched extract obtained from tilapia (*Oreochromis spp*.) has good film forming ability and a good candidate for preparation of MNs by micromolding. Olatunji *et al*. [166] reported the preparation of fish scale-based MNs showing that they can successfully penetrate porcine skin and dissolved over time. By blending this matrix with cellulose

nanocrystals, the dissolution of the needles was prevented and these were able to absorb up to 300% its own weight in water [165]. The incorporation of lidocaine into these composite MNs was successfully demonstrated in permeation studies. An increased drug permeation was observed for all four loading concentrations (2.5–10% w/w) and a pseudo steady state profile was observed for 5.0–10.0% w/w lidocaine MN loading after 30 h with an apparent flux shows increasing trends for 2.5–7.5% w/w after 36 h.

The fabrication of MNs using zein was recently reported. Zein is a plant-sourced protein which enables the preparation of glossy, tough, and greaseproof films with also low water vapor permeability and resistance to microbial attack [225]. Zein enables the preparation of structures with good mechanical performance and therefore, good penetration ability. Using ovalbumin as a model antigen, Bhatnagar *et al*. [70] showed that zein MNs provide lower microbial skin penetration when compared with hypodermic needles. Using ovalbumin coated or entrapped into the zein matrix, these MNs displayed efficient DD. Nevertheless, a greater dose of ovalbumin needs to be deposited into the needles to elicit a similar antibody response comparable with that of intradermal administration. These results support the convenient use and safety of zein MNs for transcutaneous immunization

3.3. Mechanical properties of polysaccharide and protein MNs

Polysaccharide and protein MNs are frequently evaluated by the above-mentioned axial force test. Usually these MNs exhibit force-displacement curves with no discontinuity in the process, which indicates no distinct transition point with indication of buckling failure. An overview of the data already published about mechanical tests in polysaccharide and protein MNs is summarized in Table 4. The failure force, in this case, the axial fracture force, should be above the force needed

for skin insertion to ensure proper skin insertion. Polysaccharide and protein MNs can have failure forces between 0.12 N/needle for MNs fabricated with fish scale, a collagen-enriched extract, to 0.8 N/needle for carboxymethyl cellulose MNs. As summarized in Table 4, most polysaccharide and protein MNs display a fracture force higher than 0.15 N/needle. Particularly, when comparing biopolymeric-based MNs with the other materials, namely silicon, metals and ceramics, these display lower strength. Still, in general polymers have better toughness than glass and ceramics [43]. Considering that ~0.15 N/needle are required for skin insertion, most biopolymeric MNs insert skin successfully.

To determine skin insertion, the parameter of margin of safety is usually determined. This is the ratio of MN fracture force: insertion force. To guarantee skin insertion MNs should be designed in order to increase this parameter [43].

Apart from the materials choice, the geometry, aspect ratio and humidity also affect the MNs mechanical properties. In general, the polysaccharide and protein MNs prepared hitherto present two typical shapes: pyramidal and conical. In 2008, Lee *et al*. [160] found that carboxymethyl cellulose polymeric MNs with pyramidal shapes exhibited better mechanical strength than those with conical shapes, probably due to their larger cross- sectional area at the same base width/diameter. In addition, gelatin MNs were fabricated into two different shapes, namely conical and bullet shape and after an axial force load, it was found that bullet-type MNs have higher mechanical strength. These microstructures preserve structural integrity with higher force loading and proved to be more suitable for insertion as they increase deliver of gelatin when compared with the conical ones [69].

Also, the mechanical strength of MNs with the same shape could be further improved by increasing the base width/diameter, *i.e*. decreasing the aspect ratio [135]. Notwithstanding the important

achievements reported by Lee *et al*. [160] and Park *et al*. [135] it should be noted that widening the MN base to decrease the aspect ratio may result in inefficient skin insertion. In this vein, Chen *et al*. [173] reported that increasing tip sharpness facilitates skin insertion. Using pyramidal CS MNs with a tip radius of 5 μm these authors observed an insertion depth twice than that obtained with MNs with a tip radius of 10 μm. Also, MNs with the smallest aspect ratio exhibited the highest mechanical strength and the deepest insertion depth. Furthermore, these authors reported that there is no significant difference in mechanical strength for MNs with the same aspect ratio and different dimensions and that both shapes and aspect ratios are crucial in influencing the mechanical properties of the arrays.

Owing to the fact that the exposure of MNs to air humidity can influence their mechanical properties, Wang *et al*. [131] simulated the exposure of MNs to different RH conditions with the temperature fixed at 25 °C and studied the effect on the mechanical strength and insertion ability of dissolving MNs fabricated with HA, CS and gelatin. The authors found that when analyzing the mechanical properties, the force-displacement curves showed that when the displacement went from 0 to 0.25 mm, the compression forces were of 0.40, 0.38 and 0.39 N for HA, CS and gelatin respectively. In addition, all these microneedles showed 100% insertion rate.

Then, to understand the effect of RH the samples were conditioned at different RH, from 20, 40, 60 and 80% for 30 min. For the HA MNs, compared with dried MNs, when the RH increased at 20%, the mechanical strength remained unaltered (displacement of 0.2mm with force of almost 0.4 N) but after storage at 40 and 60% RH (RH), a slight reduction was observed, with MNs presenting values closer to 0.2 N/needle with a displacement of 0.2 mm. Nevertheless, the insertion ratio was always close to 100%. However, with 80% RH the mechanical strength reduced drastically to <0.1 N /needle at 0.2 mm displacement. Regarding chitosan and gelatin MNs, the

mechanical strength and insertion ability showed little change after storage at 20% RH. Similarly, to HA MNs mentioned above, there is a slight decrease in the mechanical strength at 40 and 60% RH with successful insertion kept almost at 100%. In this case, at 80% RH MNs tips disappeared, so, the force-displacement values were not determined.

In fact, when compared with chitosan and gelatin, HA MNs were able to keep the needle-like shape. After storage at 80% RH, the structure loses strength and MNs can no longer be inserted in skin. In summary, dissolving MNs showed different changes in response to varying RH storage conditions. When conditioning samples at 20% RH the samples showed no water absorption. However, at 40, 60% and 80% RH for HA MNs, the water absorption rate increased from 0.5 to 4.9% and to 11.8%, respectively. Regarding chitosan and gelatin, the water absorption increased slightly when the samples were conditioned at 40 and 60% RH, but at 80% the absorption rates were of 8.0 and 9.6%. Overall, all these MNs can be used within 30 min after opening the packaging, which is supported by their good insertion rates.

One of the main drawbacks of using dissolvable biopolymers relies on their hygroscopic nature which will negatively impact the mechanical strength of these patches or drug stability after exposure to environment humidity. Hiraishi *et al*. [182] studied the performance of HA MNs incorporating HA, dextran and poly(vinylpyrrolidone). These devices were conditioned in a desiccator with 75% RH and after 1 week, the mechanical strength decreased 50% in relation to the dried patch, to 0.14 N/needle. The incorporation of different pharmaceutical ingredients, namely all-*trans* retinoic acid and ovalbumin also had a significant impact on the mechanical strength of MNs. Loading MNs with all-*trans* retinoic acid decreased the mechanical strength in about 50%, with the failure forces ranging between 0.04-0.056 N/needle for needles of 300 μm in height and 0.073-0.1 N/needle for MNs of 800 μm. The same tendency was observed for MNs

incorporated with ovalbumin, which presented lower mechanical strength regardless the protein concentration.

4. Conclusions and Future Perspectives

Drug delivery systems enhancing percutaneous drug absorption have progressed remarkably, one of which, the MNs patch, aids drug permeation by creating numerous microchannels in the *SC*. During the past fifteen years, the face of materials science has changed drastically and the exploitation of biopolymers for therapeutic purposes has been one of the main achievements [163,232]. Drug delivery systems enhancing percutaneous drug absorption have progressed remarkably, one of which, the MNs patch, aids drug permeation by creating numerous microchannels in the *SC*. During the past fifteen years, the face of materials science has changed drastically and the exploitation of biopolymers for therapeutic purposes has been one of the main achievements.

Remarkably, the use of polysaccharides and proteins offers a wide range of advantages due to their low toxicity, inherent biocompatibility and degradability and renewable character. However, the polysaccharide and protein-based MNs faces some limitations as well. The intrinsic variability of biopolymers, associated specially with animal and plant sourcing, coupled with its lack of standardization and changes in aesthetics during storage or processing, are some of the factors that should be noted when these enter into large scale production [232]. To overcome these challenges, proper evaluation and full characterization of biopolymers must be carried out. Another important aspect focuses on the possibility of denaturation, decomposition or contamination of these materials during their extraction and processing.

Naturally, some polysaccharides and proteins exhibit poor mechanical properties. This reflects the need for blending with other polymers [175] or nanostructures [200], and also cross-linking [218], to ensure sufficient strength to enable skin disruption. The mechanical properties can be also affected by the batch to batch variability which makes their characterization imperative before use. Polysaccharides and proteins from natural sources require purification and their technological manipulation may be more elaborate. Commercially available biopolymers can be expensive but their use for specific purposes can justify their costs.

Regarding the preparation of polysaccharide and protein MNs some aspects of research need to be re-designed. For example, for hygroscopic biopolymers, tests envisioning storage at impermeable packages should be performed. In this vein it would be possible to infer about the possibility of using these patches in countries with high RH such as the WHO Climatic Zone IV, lacking adequate accessibility and infrastructures [233]. One of the greatest advantages of MNs is the ability of self-administration. However, in mass production and self-use, a special applicator should be considered to enable appropriate administration. Using an applicator might increase the overall costs of these devices but it is important to consider the benefit of ensuring a pre-set force to guarantee skin insertion [79]. Although many active pharmaceutical ingredients are stable enough not to be affected by MNs fabrication steps, in those cases where their stability has to be taken into account, the incorporation of stabilizers into the biopolymeric formulations might be required not only to stabilize the active pharmaceutical ingredients during fabrication but to retain and provide long-lasting activity of biological substrates.

Regarding DD purposes, the real application of MNs has been delayed because the regulatory guidelines are still being gathered. However, the academia keeps delivering new though-provoking

reports on this area. This increases the difficulty in keeping up with the ever-increasing new scientific developments.

The establishment of guidelines to fabricate and evaluate the safety of MNs is imperative to guarantee standardization of a set of specifications and ensure consistent production. An excellent review of Larrañeta *et al*. [43] gives a brief summary for the establishment of microneedle specifications that need to be addressed [152,187,200,234,235]. It is important to highlight that despite the small dimensions of MNs, and near invisibility of MN tips, we should not create a false perception that these devices are totally benign and could be dismissed as possessing little or no danger. So, despite the main purpose of using MNs, we should not forget that they are penetrating skin and the material interacts with deeper skin tissue. Those micropores are expected to heal within a few hours after puncturing the skin [236]. Nevertheless, under real conditions, the micropores created in skin might be an entry for the transport of bacteria, even though the potential of bacterial infection is considerably lower than by conventional injections [237]. Still, the use of MN based DD systems should always encompass preventive disinfection measures, namely using alcoholic solutions, to reduce infection risks [236]. MNs insertion may also contribute to a pro-inflammatory microenvironment and immunological effects, especially if these are to be used on a frequent basis. Hence, it is perceived that the efficacy of MNs is partially supported by the natural mechanisms of skin for sensing and response to natural infections. The success of MNs is hindered by its ability to pierce the *SC*. Presently, there are some applicators that press MN patches against skin under a standard force value. To guarantee proper skin insertion, regulation should require that MNs should be able to insert skin at a define force value. If inserted by hand, the great variability of forces applied by different individuals might be challenging. Still, considering that are some studies addressing the average force applied by a group of volunteers, the needles should

obey at least, to the following rule: the MN patches should withstand enough force to allow skin insertion at a defined range of applied forces. To guarantee that MNs are successfully applied, they could have some responsive marker visible on the backpatch.

Another important issue (as in any other pharmaceutical formulation and/or medical device) is related with the sterilization of the MNs. This step is imperative to guarantee safety of microneedles and regulatory bodies will demand it. Sterilization might in some cases impact the stability of pharmacological agents owing to the fact that, as in any other type of pharmaceutical formulation, can induce degradation of temperature or radiation sensitive active principles.

In respect to the storage, it is envisioned that MNs should be able to be left at ambient temperatures and no need of cold chain or special environment. Hence, to guarantee quality and safety of these devices, some parameters need to be determined for each system. For example, how long will the active pharmacological agents be active within the MN array? What is the effect of temperature in the stability of the MNs systems? Answering these questions will be crucial to evaluate the effect of storage conditions over the MNs, namely their mechanical performance and biological activity.

Another important aspect focuses on the disposal of MN patches. Since there is a possibility of MNs transferring blood borne pathogens through blood or ISF, the risk of contamination with pathogens or residual drugs extends to environmental contamination if these devices are not discharged properly [237].

The future of polysaccharide and protein for the development of MNs depends largely on the development of smart devices for DD, ISF and diagnosis using nanocarriers and nanostructured polymers. Investigation has been actively studying the creation of MNs that sense pH or temperature changes. The advent of nanotechnology will possibly allow the creation of smart diagnostic MNs. As low invasive devices, MNs for diagnostic might succeed in the clinic. This

field holds huge potential and it should eventually be very successful. It is imperative to highlight that these MN devices are poised to provide an alternative to conventional administration of pharmaceuticals via oral route. Regarding the limitations of the oral route, the portability and well-known acceptability by patients, should be considered.

To conclude, elegant structures and remarkable combinations of polysaccharides and proteins have worked towards the successful delivery of different pharmacological agents using MNs, with a range of applications in several areas of human endeavor. As such, biopolymer-based MNs are playing an essential role in modern healthcare. These are poised to provide exciting breakthroughs in the realm of DD and may herald an important contribution to drug administration. In this vein, it is expected that in a few years some devices may be validated at clinical level bringing inspiration from nature into daily DD applications.

Acknowledgment

This work was developed within the scope of the project CICECO-Aveiro Institute of Materials (UID/CTM/50011/2019), financed by national funds through the FCT/MCTES and when appropriate co-financed by FEDER under the PT2020 Partnership Agreement. The research contract of C. Vilela is funded by national funds (OE), through FCT – Fundação para a Ciência e a Tecnologia, I.P., in the scope of the framework contract foreseen in the numbers 4, 5 and 6 of the article 23, of the Decree-Law 57/2016, of August 29, changed by Law 57/2017, of July 19. FCT is also acknowledged for the doctoral grant to D.F.S. Fonseca (PD/BD/115621/2016), and contract under Stimulus of Scientific Employment 2017 to C.S.R. Freire (CEECIND/00464/2017).

References

1. Anselmo, A. C.; Mitragotri, S. An overview of clinical and commercial impact of drug delivery systems. *Journal of Controlled Release* **2014**, *190*, 15–28.

2. Jain, K. K. Drug delivery systems - An overview. *Methods in Molecular Biology* **2008**, *437*, 1–50.

3. Zhang, Y.; Chan, H. F.; Leong, K. W. Advanced materials and processing for drug delivery: The past and the future. *Advanced Drug Delivery Reviews* **2013**, *65*, 104–120.

4. Wang, B.; Hu, L.; Siahaan, T. J. *Drug delivery: principles and applications*; Second.; John Wiley & Sons: Hoboken, New Jersey, 2016.

5. Goodman, L. S.; Hardman, J. G.; Limbird, L. E.; Gilman, A. G. *Goodman & Gilman's The Pharmacological Basis of Therapeutics*; 2001; Vol. 10th.

6. Wiedersberg, S.; Guy, R. H. Transdermal drug delivery: 30 + years of war and still fighting! *Journal of Controlled Release* **2014**, *190*, 150–156.

7. Raja, W. K.; Maccorkle, S.; Diwan, I. M.; Abdurrob, A.; Lu, J.; Omenetto, F. G.; Kaplan, D. L. Transdermal delivery devices: Fabrication, mechanics and drug release from silk. *Small* **2013**, *9*, 3704–3713.

8. Kurmi, B.; Tekchandani, P.; Paliwal, R.; Paliwal, S. Transdermal Drug Delivery: Opportunities and Challenges for Controlled Delivery of Therapeutic Agents Using Nanocarriers. *Current Drug Metabolism* **2017**, *18*, 1–1.

9. Park, K. Drug delivery of the future: Chasing the invisible gorilla. *Journal of Controlled Release* **2016**, *240*, 2–8.

10. Brambilla, D.; Luciani, P.; Leroux, J. C. Breakthrough discoveries in drug delivery technologies: The next 30 years. *Journal of Controlled Release* **2014**, *190*, 9–14.

11. Watkinson, A. C.; Kearney, M.-C.; Quinn, H. L.; Courtenay, A. J.; Donnelly, R. F. Future of

the transdermal drug delivery market – have we barely touched the surface? *Expert Opinion on Drug Delivery* **2016**, *13*, 523–532.

12. Donnelly, R. F.; Singh, T. R. R.; Morrow, D. I. J.; Woolfson, A. D. Transdermal Drug Delivery. In *Microneedle-Mediated Transdermal and Intradermal Drug Delivery*; John Wiley & Sons, Ltd: Chichester, UK, 2012; pp. 1–19.

13. Ita, K. B. Transdermal drug delivery: Progress and challenges. *Journal of Drug Delivery Science and Technology* **2014**, *24*, 245–250.

14. Global Transdermal Drug Delivery Market Analysis & Opportunity Outlook 2021 http://www.researchnester.com/reports/global-transdermal-drug-delivery-market-analysis-opportunity-outlook-2021/111 (accessed Jul 20, 2017).

15. Wiechers, J. W. The barrier function of the skin in relationto percutaneous absorption of drugs. *Pharm. Week Bl. Sci.* **1998**, *11*, 185–198.

16. Lipinski, C. A.; Lombardo, F.; Dominy, B. W.; Feeney, P. J. Experimental and Computational Approaches to Estimate Solubility and Permeability in Drug Discovery and Develop ment Settings. *Advanced Drug Delivery Reviews* **1997**, *23*, 3–25.

17. Rejinold, N. S.; Shin, J.-H.; Seok, H. Y.; Kim, Y.-C. Biomedical applications of microneedles in therapeutics: recent advancements and implications in drug delivery. *Expert opinion on drug delivery* **2016**, *13*, 109–31.

18. Wang, M.; Hu, L.; Xu, C. Recent advances in the design of polymeric microneedles for transdermal drug delivery and biosensing. *Lab Chip* **2017**, *17*, 1373–1387.

19. Tuan-Mahmood, T.-M. M.; McCrudden, M. T. C.; Torrisi, B. M.; McAlister, E.; Garland, M. J.; Singh, T. R. R.; Donnelly, R. F. Microneedles for intradermal and transdermal drug delivery. *European Journal of Pharmaceutical Sciences* **2013**, *50*, 623–637.

20. Larrañeta, E.; McCrudden, M. T. C.; Courtenay, A. J.; Donnelly, R. F. Microneedles: A New Frontier in Nanomedicine Delivery. *Pharmaceutical Research* **2016**, *33*, 1055–1073.

21. Donnelly, R. F.; Singh, T. R. R.; Woolfson, A. D. Microneedle-based drug delivery systems: Microfabrication, drug delivery, and safety. *Drug Delivery* **2010**, *17*, 187–207.

22. Wei-Ze, L.; Mei-Rong, H.; Jian-Ping, Z.; Yong-Qiang, Z.; Bao-Hua, H.; Ting, L.; Yong, Z. Super-short solid silicon microneedles for transdermal drug delivery applications. *International Journal of Pharmaceutics* **2010**, *389*, 122–129.

23. Khanna, P.; Luongo, K.; Strom, J. A.; Bhansali, S. Sharpening of hollow silicon microneedles to reduce skin penetration force. *Journal of Micromechanics and Microengineering* **2010**, *20*, 045011.

24. Vinayakumar, K. B.; Hegde, G. M.; Nayak, M. M.; Dinesh, N. S.; Rajanna, K. Fabrication and characterization of gold coated hollow silicon microneedle array for drug delivery. *Microelectronic Engineering* **2014**, *128*, 12–18.

25. Li, J.; Liu, B.; Zhou, Y.; Chen, Z.; Jiang, L.; Yuan, W.; Liang, L. Fabrication of a Ti porous microneedle array by metal injection molding for transdermal drug delivery. *PLoS ONE* **2017**, *12*, e0172043.

26. Hoang, M. T.; Ita, K. B.; Bair, D. A. Solid microneedles for transdermal delivery of amantadine hydrochloride and pramipexole dihydrochloride. *Pharmaceutics* **2015**, *7*, 379–396.

27. Olhero, S. M.; Lopes, E.; Ferreira, J. M. F. Fabrication of ceramic microneedles – The role of specific interactions between processing additives and the surface of oxide particles in Epoxy Gel Casting. *Journal of the European Ceramic Society* **2016**, *36*, 4131–4140.

28. Wang, P. M.; Cornwell, M.; Hill, J.; Prausnitz, M. R. Precise microinjection into skin using hollow microneedles. *Journal of Investigative Dermatology* **2006**, *126*, 1080–1087.

29. Lee, J. W.; Han, M.-R.; Park, J.-H. Polymer microneedles for transdermal drug delivery. *Journal of Drug Targeting* **2013**, *21*, 211–223.

30. Ulery, B. D.; Nair, L. S.; Laurencin, C. T. Biomedical applications of biodegradable polymers. *Journal of Polymer Science, Part B: Polymer Physics* 2011, *49*, 832–864.

31. Grund, S.; Bauer, M.; Fischer, D. Polymers in drug delivery-state of the art and future trends. *Advanced Engineering Materials* **2011**, *13*, B61–B87.

32. Kumbar, S.; Laurencin, C.; Deng, M. *Natural and Synthetic Biomedical Polymers*; Elsevier Science, 2014.

33. Tibbitt, M. W.; Rodell, C. B.; Burdick, J. A.; Anseth, K. S. Progress in material design for biomedical applications. *Proceedings of the National Academy of Sciences* **2015**, *112*, 14444–14451.

34. Wei, Q.; Haag, R. Universal polymer coatings and their representative biomedical applications. *Materials Horizons* **2015**, *2*, 567–577.

35. Wang, M.; Hu, L.; Xu, C. Recent advances in the design of polymeric microneedles for transdermal drug delivery and biosensing. *Lab Chip* **2017**, *17*, 1373–1387.

36. Niaounakis, M. *Biopolymers : applications and trends*; Elsevier, 2016.

37. Thanou, M.; Verhoef, J. .; Junginger, H. . Chitosan and its derivatives as intestinal absorption enhancers. *Advanced Drug Delivery Reviews* **2001**, *50*, S91–S101.

38. Chang, H.; Zheng, M.; Yu, X.; Than, A.; Seeni, R. Z.; Kang, R.; Tian, J.; Khanh, D. P.; Liu, L.; Chen, P.; Xu, C. A Swellable Microneedle Patch to Rapidly Extract Skin Interstitial Fluid for Timely Metabolic Analysis. *Advanced Materials* **2017**, *29*, 1702243.

39. Yu, W.; Jiang, G.; Liu, D.; Li, L.; Chen, H.; Liu, Y.; Huang, Q.; Tong, Z.; Yao, J.; Kong, X. Fabrication of biodegradable composite microneedles based on calcium sulfate and gelatin for

transdermal delivery of insulin. *Materials Science & Engineering C* **2017**, *71*, 725–734.

40. Tsai, Y.-S.; Chen, M.-Y.; Lan, S.-K.; Tsai, H.-T.; Chen, M.-C.; Tzai, T.-S. Transdermal delivery of leuprolide acetate with chitosan microneedles: A promising tool for androgen deprivation therapy. *European Urology Supplements* **2017**, *16*, e1304.

41. Ita, K. Ceramic microneedles and hollow microneedles for transdermal drug delivery: Two decades of research. *Journal of Drug Delivery Science and Technology* **2018**, *44*, 314–322.

42. Ita, K. Transdermal delivery of drugs with microneedles: Strategies and outcomes. *Journal of Drug Delivery Science and Technology* **2015**, *29*, 16–23.

43. Larrañeta, E.; Lutton, R. E. M.; Woolfson, A. D.; Donnelly, R. F. Microneedle arrays as transdermal and intradermal drug delivery systems: Materials science, manufacture and commercial development. *Materials Science and Engineering R: Reports* **2016**, *104*, 1–32.

44. Cahill, E. M.; Ocearbhaill, E. D. Toward Biofunctional Microneedles for Stimulus Responsive Drug Delivery. *Bioconjugate Chemistry* **2015**, *26*, 1289–1296.

45. Ye, Y.; Yu, J.; Wen, D.; Kahkoska, A. R.; Gu, Z. Polymeric microneedles for transdermal protein delivery. *Advanced Drug Delivery Reviews* **2018**, *127*, 106–118.

46. Gerstel, M. S.; Place, V. A. Drug delivery device 1976.

47. Henry, S.; McAllister, D. V.; Allen, M. G.; Prausnitz, M. R.; Gaugler, R.; Trimmer, W. Microfabricated Microneedles: A Novel Approach to Transdermal Drug Delivery. *Journal of Pharmaceutical Sciences* **1998**, *87*, 922–925.

48. Ikeno, F.; Lyons, J.; Kaneda, H.; Baluom, M.; Benet, L. Z.; Rezaee, M. Novel percutaneous adventitial drug delivery system for regional vascular treatment. *Catheterization and Cardiovascular Interventions* **2004**, *63*, 222–230.

49. Reed, M. L.; Wu, C.; Kneller, J.; Watkins, S.; Vorp, D. A.; Nadeem, A.; Weiss, L. E.; Rebello,

K.; Mescher, M.; Conrad Smith, A. J.; Rosenblum, W.; Feldman, M. D. Micromechanical devices for intravascular drug delivery. *Journal of Pharmaceutical Sciences* **1998**, *87*, 1387–1394.

50. Donnelly, R. F.; Singh, T. R. R.; Woolfson, A. D.; Raj Singh, T. R.; Woolfson, A. D. Microneedle-based drug delivery systems: Microfabrication, drug delivery, and safety. *Drug delivery* **2010**, *17*, 187–207.

51. Birchall, J. C.; Clemo, R.; Anstey, A.; John, D. N. Microneedles in clinical practice-an exploratory study into the opinions of healthcare professionals and the public. *Pharmaceutical Research* **2011**, *28*, 95–106.

52. Ashraf, M. W.; Tayyaba, S.; Afzulpurkar, N. Micro Electromechanical Systems (MEMS) based microfluidic devices for biomedical applications. *International Journal of Molecular Sciences* 2011, *12*, 3648–3704.

53. Jung, P. G.; Lee, T. W.; Oh, D. J.; Hwang, S. J.; Jung, I. D.; Lee, S. Mi.; Ko, J. S. Nickel microneedles fabricated by sequential copper and nickel electroless plating and copper chemical wet etching. *Sensors and Materials* **2008**, *20*, 45–53.

54. Chandrasekaran, S.; Frazier, A. B. Characterization of surface micromachined metallic microneedles. *Journal of Microelectromechanical Systems* **2003**, *12*, 289–295.

55. Park, J. H.; Yoon, Y. K.; Choi, S. O.; Prausnitz, M. R.; Allen, M. G. Tapered conical polymer microneedles fabricated using an integrated lens technique for transdermal drug delivery. *IEEE Transactions on Biomedical Engineering* **2007**, *54*, 903–913.

56. Lee, I.-C.; He, J.-S.; Tsai, M.-T.; Lin, K.-C. Fabrication of a novel partially dissolving polymer microneedle patch for transdermal drug delivery. *Journal of Materials Chemistry B* **2015**, *3*, 276–285.

57. Cole, G.; McCaffrey, J.; Ali, A. A.; McBride, J. W.; McCrudden, C. M.; Vincente-Perez, E.

M.; Donnelly, R. F.; McCarthy, H. O. Dissolving microneedles for DNA vaccination: Improving functionality via polymer characterization and RALA complexation. *Human Vaccines and Immunotherapeutics* **2017**, *13*, 50–62.

58. Chen, M. C.; Ling, M. H.; Kusuma, S. J. Poly-γ-glutamic acid microneedles with a supporting structure design as a potential tool for transdermal delivery of insulin. *Acta Biomaterialia* **2015**, *24*, 106–116.

59. Marin, A.; Andrianov, A. K. Carboxymethylcellulose–Chitosan-coated microneedles with modulated hydration properties. *Journal of Applied Polymer Science* **2011**, *121*, 395–401.

60. Chen, M.-C.; Huang, S.-F.; Lai, K.-Y.; Ling, M.-H. Fully embeddable chitosan microneedles as a sustained release depot for intradermal vaccination. *Biomaterials* **2013**, *34*, 3077–3086.

61. Huh, I.; Kim, S.; Yang, H.; Jang, M.; Kang, G.; Jung, H. Effects of two droplet-based dissolving microneedle manufacturing methods on the activity of encapsulated epidermal growth factor and ascorbic acid. *European Journal of Pharmaceutical Sciences* **2018**, *114*, 285–292.

62. Demir, Y. K.; Akan, Z.; Kerimoglu, O. Characterization of Polymeric Microneedle Arrays for Transdermal Drug Delivery. *PLoS ONE* **2013**, *8*, e77289.

63. Lau, S.; Fei, J.; Liu, H.; Chen, W.; Liu, R. Multilayered pyramidal dissolving microneedle patches with flexible pedestals for improving effective drug delivery. *Journal of Controlled Release* **2017**, *265*, 113–119.

64. Choi, J. T.; Park, S. J.; Park, J. H. Microneedles containing cross-linked hyaluronic acid particulates for control of degradation and swelling behaviour after administration into skin. *Journal of Drug Targeting* **2018**, *26*, 1–11.

65. Zhang, J. N.; Chen, B. Z.; Ashfaq, M.; Zhang, X. P.; Guo, X. D. Development of a BDDE-crosslinked hyaluronic acid based microneedles patch as a dermal filler for anti-ageing treatment.

Journal of Industrial and Engineering Chemistry **2018**, *65*, 363–369.

66. Lee, I. C.; Lin, W. M.; Shu, J. C.; Tsai, S. W.; Chen, C. H.; Tsai, M. T. Formulation of two-layer dissolving polymeric microneedle patches for insulin transdermal delivery in diabetic mice. *Journal of Biomedical Materials Research - Part A* **2017**, *105*, 84–93.

67. Park, Y. H.; Ha, S. K.; Choi, I.; Kim, K. S.; Park, J.; Choi, N.; Kim, B.; Sung, J. H. Fabrication of degradable carboxymethyl cellulose (CMC) microneedle with laser writing and replica molding process for enhancement of transdermal drug delivery. *Biotechnology and Bioprocess Engineering* **2016**, *21*, 110–118.

68. Yu, W.; Jiang, G.; Liu, D.; Li, L.; Tong, Z.; Yao, J.; Kong, X. Transdermal delivery of insulin with bioceramic composite microneedles fabricated by gelatin and hydroxyapatite. *Materials Science and Engineering C* **2017**, *73*, 425–428.

69. An, S. M.; Seong, K. Y.; Yim, S. G.; Hwang, Y. J.; Bae, S. H.; Yang, S. Y.; An, B. S. Intracutaneous delivery of gelatins induces lipolysis and suppresses lipogenesis of adipocytes. *Acta Biomaterialia* **2017**, *67*, 238–247.

70. Bhatnagar, S.; Chawla, S. R.; Kulkarni, O. P.; Venuganti, V. V. K. Zein Microneedles for Transcutaneous Vaccine Delivery: Fabrication, Characterization, and in Vivo Evaluation Using Ovalbumin as the Model Antigen. *ACS Omega* **2017**, *2*, 1321–1332.

71. Ding, D.; Pan, J.; Lim, S. H.; Amini, S.; Kang, L.; Miserez, A. Squid suckerin microneedle arrays for tunable drug release. *Journal of Materials Chemistry B* **2017**, *5*, 8467–8478.

72. Nguyen, H. X.; Banga, A. K. Fabrication, characterization and application of sugar microneedles for transdermal drug delivery. *Therapeutic Delivery* **2017**, *8*, 249–264.

73. Loizidou, E. Z.; Williams, N. A.; Barrow, D. A.; Eaton, M. J.; McCrory, J.; Evans, S. L.; Allender, C. J. Structural characterisation and transdermal delivery studies on sugar microneedles:

Experimental and finite element modelling analyses. *European Journal of Pharmaceutics and Biopharmaceutics* **2015**, *89*, 224–231.

74. Chu, L. Y.; Choi, S.; Prausnitz, M. R. Fabrication of dissolving polymer microneedles for controlled drug encapsulation and delivery: bubble and pedestal microneedle designs. *Journal of pharmaceutical sciences* **2010**, *99*, 4228–4238.

75. Sullivan, S. P.; Murthy, N.; Prausnitz, M. R. Minimally invasive protein delivery with rapidly dissolving polymer microneedles. *Advanced Materials* **2008**, *20*, 933–938.

76. Lee, K.; Lee, C. Y.; Jung, H. Dissolving microneedles for transdermal drug administration prepared by stepwise controlled drawing of maltose. *Biomaterials* **2011**, *32*, 3134–3140.

77. Ko, P. T.; Lee, I. C.; Chen, M. C.; Tsai, S. W. Polymer microneedles fabricated from PCL and PCL/PEG blends for transdermal delivery of hydrophilic compounds. *Journal of the Taiwan Institute of Chemical Engineers* **2015**, *51*, 1–8.

78. Prausnitz, M. R. Microneedles for transdermal drug delivery. *Advanced Drug Delivery Reviews* **2004**, *56*, 581–587.

79. van der Maaden, K.; Sekerdag, E.; Jiskoot, W.; Bouwstra, J. Impact-Insertion Applicator Improves Reliability of Skin Penetration by Solid Microneedle Arrays. *The AAPS Journal* **2014**, *16*, 681–684.

80. Witting, M.; Obst, K.; Pietzsch, M.; Friess, W.; Hedtrich, S. Feasibility study for intraepidermal delivery of proteins using a solid microneedle array. *International Journal of Pharmaceutics* **2015**, *486*, 52–58.

81. Chen, Y.; Chen, B. Z.; Wang, Q. L.; Jin, X.; Guo, X. D. Fabrication of coated polymer microneedles for transdermal drug delivery. *Journal of Controlled Release* **2016**.

82. Donnelly, R. F.; Majithiya, R.; Singh, T. R. R.; Morrow, D. I. J. J.; Garland, M. J.; Demir, Y.

K.; Migalska, K.; Ryan, E.; Gillen, D.; Scott, C. J.; Woolfson, A. D. Design, optimization and characterisation of polymeric microneedle arrays prepared by a novel laser-based micromoulding technique. *Pharmaceutical Research* **2011**, *28*, 41–57.

83. Demuth, P. C.; Moon, J. J.; Suh, H.; Hammond, P. T.; Irvine, D. J. Releasable layer-by-layer assembly of stabilized lipid nanocapsules on microneedles for enhanced transcutaneous vaccine delivery. *ACS Nano* **2012**, *6*, 8041–8051.

84. van der Maaden, K.; Sekerdag, E.; Schipper, P.; Kersten, G.; Jiskoot, W.; Bouwstra, J. Layer-by-Layer Assembly of Inactivated Poliovirus and N-Trimethyl Chitosan on pH-Sensitive Microneedles for Dermal Vaccination. *Langmuir* **2015**, *31*, 8654–8660.

85. Wang, C.; Ye, Y.; Hochu, G. M.; Sadeghifar, H.; Gu, Z. Enhanced Cancer Immunotherapy by Microneedle Patch-Assisted Delivery of Anti-PD1 Antibody. *Nano Letters* **2016**, *16*, 2334–2340.

86. Donnelly, R. F.; McCrudden, M. T. C. C.; Alkilani, A. Z.; Larrañeta, E.; McAlister, E.; Courtenay, A. J.; Kearney, M.-C. C.; Singh, T. R. R.; McCarthy, H. O.; Kett, V. L.; Raj Singh, T. R.; McCarthy, H. O.; Kett, V. L.; Caffarel-Salvador, E.; Al-Zahrani, S.; Woolfson, A. D.; Singh, T. R. R.; McCarthy, H. O.; Kett, V. L.; Raj Singh, T. R.; McCarthy, H. O.; Kett, V. L.; Caffarel-Salvador, E.; Al-Zahrani, S.; Woolfson, A. D. Hydrogel-forming microneedles prepared from "super swelling" polymers combined with lyophilised wafers for transdermal drug delivery. *PLoS ONE* **2014**, *9*, e111547.

87. Khumpuang, S.; Horade, M.; Fujioka, K.; Sugiyama, S. Geometrical strengthening and tip-sharpening of a microneedle array fabricated by X-ray lithography. *Microsystem Technologies* **2007**, *13*, 209–214.

88. Patel, S. R.; Lin, A. S. P.; Edelhauser, H. F.; Prausnitz, M. R. Suprachoroidal drug delivery to the back of the eye using hollow microneedles. *Pharmaceutical Research* **2011**, *28*, 166–176.

89. Roxhed, N.; Samel, B.; Nordquist, L.; Griss, P.; Stemme, G. Painless drug delivery through microneedle-based transdermal patches featuring active infusion. *IEEE Transactions on Biomedical Engineering* **2008**, *55*, 1063–1071.

90. Wang, P. M.; Cornwell, M.; Hill, J.; Prausnitz, M. R. Precise Microinjection into Skin Using Hollow Microneedles. *The Journal of investigative dermatology* **2006**, *126*, 1080–7.

91. Davis, S. P.; Martanto, W.; Allen, M. G.; Prausnitz, M. R. Hollow metal microneedles for insulin delivery to diabetic rats. *IEEE Transactions on Biomedical Engineering* **2005**, *52*, 909–915.

92. Gardeniers, H. J. G. E.; Luttge, R.; Berenschot, E. J. W.; De Boer, M. J.; Yeshurun, S. Y.; Hefetz, M.; Van't Oever, R.; Van Den Berg, A. Silicon micromachined hollow microneedles for transdermal liquid transport. *Journal of Microelectromechanical Systems* **2003**, *12*, 855–862.

93. Griss, P.; Stemme, G. Side-opened out-of-plane microneedles for microfluidic transdermal liquid transfer. *Journal of Microelectromechanical Systems* **2003**, *12*, 296–301.

94. Martanto, W.; Moore, J. S.; Couse, T.; Prausnitz, M. R. Mechanism of fluid infusion during microneedle insertion and retraction. *Journal of Controlled Release* **2006**, *112*, 357–361.

95. Akers, M. J. Excipient-drug interactions in parenteral formulations. *Journal of Pharmaceutical Sciences* **2002**, *91*, 2283–2300.

96. Donnelly, R.; McCarron, P.; Morrow, D.; Morrissey, A.; Woolfson, D. Microneedles/Delivery Device and Method. **2007**.

97. Donnelly, R. F.; Singh, T. R. R.; Garland, M. J.; Migalska, K.; Majithiya, R.; McCrudden, C. M.; Kole, P. L.; Mahmood, T. M. T.; McCarthy, H. O.; Woolfson, A. D. Hydrogel-forming microneedle arrays for enhanced transdermal drug delivery. *Advanced Functional Materials* **2012**, *22*, 4879–4890.

98. Yang, S.; Feng, Y.; Zhang, L.; Chen, N.; Yuan, W.; Jin, T. A scalable fabrication process of polymer microneedles. *International Journal of Nanomedicine* **2012**, *7*, 1415–1422.

99. Sammoura, F.; Kang, J.; Heo, Y. M.; Jung, T.; Lin, L. Polymeric microneedle fabrication using a microinjection molding technique. *Microsystem Technologies* **2007**, *13*, 517–522.

100. Koch, B.; Rubino, I.; Quan, F.-S.; Yoo, B.; Choi, H.-J. Microfabrication for Drug Delivery. *Materials* **2016**, *9*, 646.

101. Banks, D. Microengineering, MEMS, and Interfacing: A practical Guide. In *Microengineering, MEMS, and Interfacing: A practical Guide*; Dekker Mechanical Engineering; CRC Press, 2006; Vol. 199, pp. 1–10.

102. *Fundamentals of Microfabrication: The Science of Miniaturization, Second Edition - Marc J. Madou - Google Books*.

103. Verbaan, F. J.; Bal, S. M.; van den Berg, D. J.; Groenink, W. H. H.; Verpoorten, H.; Lüttge, R.; Bouwstra, J. A. Assembled microneedle arrays enhance the transport of compounds varying over a large range of molecular weight across human dermatomed skin. *Journal of Controlled Release* **2007**, *117*, 238–245.

104. Rajabi, M.; Roxhed, N.; Shafagh, R. Z.; Haraldson, T.; Fischer, A. C.; Van Der Wijngaart, W.; Stemme, G.; Niklaus, F. Flexible and stretchable microneedle patches with integrated rigid stainless steel microneedles for transdermal biointerfacing. *PLoS ONE* **2016**, *11*, e0166330.

105. Martanto, W.; Davis, S. P.; Holiday, N. R.; Wang, J.; Gill, H. S.; Prausnitz, M. R. Transdermal delivery of insulin using microneedles in vivo. *Pharmaceutical Research* **2004**, *21*, 947–952.

106. Lee, K.; Lee, H. C.; Lee, D. S.; Jung, H. Drawing lithography: Three-dimensional fabrication of an ultrahigh-aspect-ratio microneedle. *Advanced Materials* **2010**, *22*, 483–486.

107. Bystrova, S.; Luttge, R. Micromolding for ceramic microneedle arrays. *Microelectronic*

Engineering **2011**, *88*, 1681–1684.

108. Papautsky, I.; Peterson, E. T. K. Micromolding. In *Encyclopedia of Microfluidics and Nanofluidics*; Springer US: Boston, MA, 2014; pp. 1–17.

109. McCrudden, M. T. C.; Alkilani, A. Z.; Courtenay, A. J.; McCrudden, C. M.; McCloskey, B.; Walker, C.; Alshraiedeh, N.; Lutton, R. E. M.; Gilmore, B. F.; Woolfson, A. D.; Donnelly, R. F. Considerations in the sterile manufacture of polymeric microneedle arrays. *Drug Delivery and Translational Research* **2014**, *5*, 3–14.

110. Lin, Y.-H.; Lee, I.-C.; Hsu, W.-C.; Hsu, C.-H.; Chang, K.-P.; Gao, S.-S. Rapid fabrication method of a microneedle mold with controllable needle height and width. *Biomedical Microdevices* **2016**, *18*, 85.

111. Jin, C. Y.; Han, M. H.; Lee, S. S.; Choi, Y. H. Mass producible and biocompatible microneedle patch and functional verification of its usefulness for transdermal drug delivery. *Biomedical Microdevices* **2009**, *11*, 1195–1203.

112. Lippmann, J. M.; Geiger, E. J.; Pisano, A. P. Polymer investment molding: Method for fabricating hollow, microscale parts. *Sensors and Actuators, A: Physical* **2007**, *134*, 2–10.

113. Kim, J. D.; Kim, M.; Yang, H.; Lee, K.; Jung, H. Droplet-born air blowing: Novel dissolving microneedle fabrication. *Journal of Controlled Release* **2013**, *170*, 430–436.

114. Esposito, E.; Ruggiero, F.; Vecchione, R.; Netti, A. P. Room Temperature Consolidation of a Porous Poly(lactic-co-glycolic acid) Matrix by the Addition of Maltose to the Water-in-Oil Emulsion. *Materials* 2016, *9*.

115. Vecchione, R.; Coppola, S.; Esposito, E.; Casale, C.; Vespini, V.; Grilli, S.; Ferraro, P.; Netti, P. A. Electro-Drawn Drug-Loaded Biodegradable Polymer Microneedles as a Viable Route to Hypodermic Injection. *Advanced Functional Materials* **2014**, *24*, 3515–3523.

116. Caliò, A.; Dardano, P.; Di Palma, V.; Bevilacqua, M. F.; Di Matteo, A.; Iuele, H.; De Stefano, L. Polymeric microneedles based enzymatic electrodes for electrochemical biosensing of glucose and lactic acid. *Sensors and Actuators B: Chemical* **2016**, *236*, 343–349.

117. Dardano, P.; Caliò, A.; Di Palma, V.; Bevilacqua, F. M.; Di Matteo, A.; De Stefano, L. A Photolithographic Approach to Polymeric Microneedles Array Fabrication. *Materials* 2015, *8*.

118. Johnson, A. R.; Caudill, C. L.; Tumbleston, J. R.; Bloomquist, C. J.; Moga, K. A.; Ermoshkin, A.; Shirvanyants, D.; Mecham, S. J.; Luft, J. C.; DeSimone, J. M. Single-Step Fabrication of Computationally Designed Microneedles by Continuous Liquid Interface Production. *PLOS ONE* **2016**, *11*, e0162518.

119. Appuhamillage, G. A.; Reagan, J. C.; Khorsandi, S.; Davidson, J. R.; Voit, W.; Smaldone, R. A. 3D printed remendable polylactic acid blends with uniform mechanical strength enabled by a dynamic Diels-Alder reaction. *Polymer Chemistry* **2017**, *8*, 2087–2092.

120. Döpp, A.; Guillaume, E.; Thaury, C.; Gautier, J.; Ta Phuoc, K.; Malka, V. 3D printing of gas jet nozzles for laser-plasma accelerators. *Review of Scientific Instruments* **2016**, *87*, 073505.

121. Matteucci, M.; Fanetti, M.; Casella, M.; Gramatica, F.; Gavioli, L.; Tormen, M.; Grenci, G.; De Angelis, F.; Di Fabrizio, E. Poly vinyl alcohol re-usable masters for microneedle replication. *Microelectronic Engineering* **2009**, *86*, 752–756.

122. Cha, K. J.; Kim, T.; Park, S. J.; Kim, D. S. Simple and cost-effective fabrication of solid biodegradable polymer microneedle arrays with adjustable aspect ratio for transdermal drug delivery using acupuncture microneedles. *Journal of Micromechanics and Microengineering* **2014**, *24*, 115015.

123. Moon, S. J.; Lee, S. S.; Lee, H. S.; Kwon, T. H. Fabrication of microneedle array using LIGA and hot embossing process. In *Microsystem Technologies*; Springer-Verlag, 2005; Vol. 11, pp.

311–318.

124. Han, M.; Kim, D. K.; Kang, S. H.; Yoon, H. R.; Kim, B. Y.; Lee, S. S.; Kim, K. D.; Lee, H. G. Improvement in antigen-delivery using fabrication of a grooves-embedded microneedle array. *Sensors and Actuators, B: Chemical* **2009**, *137*, 274–280.

125. Wang, Q. L.; Zhang, X. P.; Chen, B. Z.; Guo, X. D. Dissolvable layered microneedles with core-shell structures for transdermal drug delivery. *Materials Science and Engineering C* **2018**, *83*, 143–147.

126. Latza, V.; Guerette, P. A.; Ding, D.; Amini, S.; Kumar, A.; Schmidt, I.; Keating, S.; Oxman, N.; Weaver, J. C.; Fratzl, P.; Miserez, A.; Masic, A. Multi-scale thermal stability of a hard thermoplastic protein-based material. *Nature Communications* **2015**, *6*.

127. Yang, H.; Kim, S.; Kang, G.; Lahiji, S. F.; Jang, M.; Kim, Y. M.; Kim, J.-M. M.; Cho, S.-N. N.; Jung, H. Centrifugal Lithography: Self-Shaping of Polymer Microstructures Encapsulating Biopharmaceutics by Centrifuging Polymer Drops. *Advanced Healthcare Materials* **2017**, *6*, 1700326.

128. Guo, N.; Leu, M. C. Additive manufacturing: Technology, applications and research needs. *Frontiers of Mechanical Engineering* **2013**, *8*, 215–243.

129. Luzuriaga, M. A.; Berry, D. R.; Reagan, J. C.; Smaldone, R. A.; Gassensmith, J. J. Biodegradable 3D printed polymer microneedles for transdermal drug delivery. *Lab on a Chip* **2018**, *18*, 1223–1230.

130. Jung-Hwan, P.; Mark, P. Analysis of mechanical failure of polymer microneedles by axial force. *Journal of the Korean Physical Society* **2010**, *56*, 1223.

131. Wang, Q. L.; Ren, J. W.; Chen, B. Z.; Jin, X.; Zhang, C. Y.; Guo, X. D. Effect of humidity on mechanical properties of dissolving microneedles for transdermal drug delivery. *Journal of*

Industrial and Engineering Chemistry **2018**, *59*, 251–258.

132. Davis, S. P.; Landis, B. J.; Adams, Z. H.; Allen, M. G.; Prausnitz, M. R. Insertion of microneedles into skin: Measurement and prediction of insertion force and needle fracture force. *Journal of Biomechanics* **2004**, *37*, 1155–1163.

133. Zahn, J.; Talbot, N.; Liepmann, D.; Pisano, A. Microfabricated polysilicon microneedles for minimally invasive biomedical devices. *Biomedical microdevices* **2000**, *2*, 295–303.

134. Khanna, P.; Luongo, K.; Strom, J. A.; Bhansali, S. Sharpening of hollow silicon microneedles to reduce skin penetration force. *Journal of Micromechanics and Microengineering* **2010**, *20*, 045011.

135. Park, J.-H. H.; Allen, M. G.; Prausnitz, M. R. Biodegradable polymer microneedles: Fabrication, mechanics and transdermal drug delivery. *Journal of Controlled Release* **2005**, *104*, 51–66.

136. Gittard, S. D.; Chen, B.; Xu, H.; Ovsianikov, A.; Chichkov, B. N.; Monteiro-Riviere, N. A.; Narayan, R. J. The Effects of Geometry on Skin Penetration and Failure of Polymer Microneedles. *Journal of adhesion science and technology* **2013**, *27*, 227–243.

137. Khanna, P.; Luongo, K.; Strom, J. A.; Bhansali, S. Sharpening of hollow silicon microneedles to reduce skin penetration force. *Journal of Micromechanics and Microengineering* **2010**, *20*, 045011.

138. Roxhed, N.; Gasser, T. C.; Griss, P.; Holzapfel, G. A.; Stemme, Gö. Penetration-enhanced ultrasharp microneedles and prediction on skin interaction for efficient transdermal drug delivery. *Journal of Microelectromechanical Systems* **2007**, *16*, 1429–1440.

139. Lhernould, M. S.; Gobillon, C.; Lambert, P. Microneedle array penetration tests: Understanding the "bed of nails" phenomenon. *ONdrugDelivery* **2013**, *40*, 29–32.

140. Bal, S. M.; Caussin, J.; Pavel, S.; Bouwstra, J. A. In vivo assessment of safety of microneedle arrays in human skin. *European Journal of Pharmaceutical Sciences* **2008**, *35*, 193–202.

141. Donnelly, R. F.; Garland, M. J.; Morrow, D. I. J.; Migalska, K.; Singh, T. R. R.; Majithiya, R.; Woolfson, A. D. Optical coherence tomography is a valuable tool in the study of the effects of microneedle geometry on skin penetration characteristics and in-skin dissolution. *Journal of Controlled Release* **2010**, *147*, 333–341.

142. Gomaa, Y. A.; Garland, M. J.; McInnes, F.; El-Khordagui, L. K.; Wilson, C.; Donnelly, R. F. Laser-engineered dissolving microneedles for active transdermal delivery of nadroparin calcium. *European Journal of Pharmaceutics and Biopharmaceutics* **2012**, *82*, 299–307.

143. Ito, Y.; Nakahigashi, T.; Yoshimoto, N.; Ueda, Y.; Hamasaki, N.; Takada, K. Transdermal Insulin Application System with Dissolving Microneedles. *Diabetes Technology & Therapeutics* **2012**, *14*, 891–899.

144. Abd, E.; Yousef, S. A.; Pastore, M. N.; Telaprolu, K.; Mohammed, Y. H.; Namjoshi, S.; Grice, J. E.; Roberts, M. S. Skin models for the testing of transdermal drugs. *Clinical Pharmacology: Advances and Applications* **2016**, *8*, 163–176.

145. Larrañeta, E.; Moore, J.; Vicente-Pérez, E. M.; González-Vázquez, P.; Lutton, R.; Woolfson, A. D.; Donnelly, R. F. A proposed model membrane and test method for microneedle insertion studies. *International Journal of Pharmaceutics* **2014**, *472*, 65–73.

146. Liu, S.; Wu, D.; Quan, Y. S.; Kamiyama, F.; Kusamori, K.; Katsumi, H.; Sakane, T.; Yamamoto, A. Improvement of Transdermal Delivery of Exendin-4 Using Novel Tip-Loaded Microneedle Arrays Fabricated from Hyaluronic Acid. *Molecular Pharmaceutics* **2016**, *13*, 272–279.

147. Kang, G.; Tu, T. N. T.; Kim, S.; Yang, H.; Jang, M.; Jo, D.; Ryu, J.; Baek, J.; Jung, H.

Adenosine-loaded dissolving microneedle patches to improve skin wrinkles, dermal density, elasticity and hydration. *International Journal of Cosmetic Science* **2018**, *40*, 199–206.

148. Medhi, P.; Olatunji, O.; Nayak, A.; Uppuluri, C. T.; Olsson, R. T.; Nalluri, B. N.; Das, D. B. Lidocaine-loaded fish scale-nanocellulose biopolymer composite microneedles. *AAPS PharmSciTech* **2017**, *18*, 1488–1494.

149. Tsioris, K.; Raja, W. K.; Pritchard, E. M.; Panilaitis, B.; Kaplan, D. L.; Omenetto, F. G. Fabrication of silk microneedles for controlled-release drug delivery. *Advanced Functional Materials* **2012**, *22*, 330–335.

150. Lee, J. Y.; Park, S. H.; Seo, I. H.; Lee, K. J.; Ryu, W. H. Rapid and repeatable fabrication of high A/R silk fibroin microneedles using thermally-drawn micromolds. *European Journal of Pharmaceutics and Biopharmaceutics* **2015**, *94*, 11–19.

151. Yin, Z.; Kuang, D.; Wang, S.; Zheng, Z.; Yadavalli, V. K.; Lu, S. Swellable silk fibroin microneedles for transdermal drug delivery. *International Journal of Biological Macromolecules* **2018**, *106*, 48–56.

152. Lee, Y.; Dugansani, S. R.; Jeon, S. H.; Hwang, S. H.; Kim, J. H.; Park, S. H.; Jeong, J. H. Drug-Delivery System Based on Salmon DNA Nano- and Micro-Scale Structures. *Scientific Reports* **2017**, *7*.

153. Park, Y.; Kim, B. Skin permeability of compounds loaded within dissolving microneedles dependent on composition of sodium hyaluronate and carboxymethyl cellulose. *Korean Journal of Chemical Engineering* **2017**, *34*, 133–138.

154. Park, Y.; Kim, B. Skin permeability of compounds loaded within dissolving microneedles dependent on composition of sodium hyaluronate and carboxymethyl cellulose. *Korean J. Chem. Eng* **2017**, *34*, 133–138.

155. Lee, I. C.; Lin, W. M.; Shu, J. C.; Tsai, S. W.; Chen, C. H.; Tsai, M. T. Formulation of two-layer dissolving polymeric microneedle patches for insulin transdermal delivery in diabetic mice. *Journal of Biomedical Materials Research - Part A* **2017**, *105*, 84–93.

156. Shelke, N. B.; James, R.; Laurencin, C. T.; Kumbar, S. G. Polysaccharide biomaterials for drug delivery and regenerative engineering. *Polymers for Advanced Technologies* **2014**, *25*, 448–460.

157. Markovsky, E.; Baabur-Cohen, H.; Eldar-Boock, A.; Omer, L.; Tiram, G.; Ferber, S.; Ofek, P.; Polyak, D.; Scomparin, A.; Satchi-Fainaro, R. Administration, distribution, metabolism and elimination of polymer therapeutics. *Journal of Controlled Release* **2012**, *161*, 446–460.

158. Mansour, H. M.; Sohn, M. J.; Al-Ghananeem, A.; DeLuca, P. P. Materials for pharmaceutical dosage forms: Molecular pharmaceutics and controlled release drug delivery aspects. *International Journal of Molecular Sciences* **2010**, *11*, 3298–3322.

159. Alam, M. T.; Parvez, N.; Sharma, P. K. FDA-Approved Natural Polymers for Fast Dissolving Tablets. *Journal of Pharmaceutics* **2014**, *2014*, 1–6.

160. Lee, J. W.; Park, J.-H. H.; Prausnitz, M. R. Dissolving microneedles for transdermal drug delivery. *Biomaterials* **2008**, *29*, 2113–2124.

161. Quinn, H. L.; Bonham, L.; Hughes, C. M.; Donnelly, R. F. Design of a Dissolving Microneedle Platform for Transdermal Delivery of a Fixed-Dose Combination of Cardiovascular Drugs. *Journal of Pharmaceutical Sciences* **2015**, *104*, 3490–3500.

162. Fukushima, K.; Ise, A.; Morita, H.; Hasegawa, R.; Ito, Y.; Sugioka, N.; Takada, K. Two-layered dissolving microneedles for percutaneous delivery of peptide/protein drugs in rats. *Pharmaceutical Research* **2011**, *28*, 7–21.

163. Tang, Z.; He, C.; Tian, H.; Ding, J.; Hsiao, B. S.; Chu, B.; Chen, X. Polymeric nanostructured

materials for biomedical applications. *Progress in Polymer Science* 2016, *60*, 86–128.

164. Ito, Y.; Kashiwara, S.; Fukushima, K.; Takada, K. Two-layered dissolving microneedles for percutaneous delivery of sumatriptan in rats. *Drug Development and Industrial Pharmacy* **2011**, *37*, 1387–1393.

165. Olatunji, O.; Olsson, R. T. Microneedles from Fishscale-Nanocellulose Blends Using Low Temperature Mechanical Press Method. *Pharmaceutics* **2015**, *7*, 363–378.

166. Olatunji, O.; Igwe, C. C.; Ahmed, A. S.; Alhassan, D. O. A. A.; Asieba, Gg. O.; Diganta, B. Das Microneedles from fish scale biopolymer. *Journal of Applied Polymer Science* **2014**, *131*, n/a-n/a.

167. You, X.; Chang, J. H.; Ju, B. K.; Pak, J. J. Rapidly dissolving fibroin microneedles for transdermal drug delivery. *Materials Science and Engineering C* **2011**, *31*, 1632–1636.

168. Park, Y.; Kim, K. S.; Chung, M.; Sung, J. H.; Kim, B. Fabrication and characterization of dissolving microneedle arrays for improving skin permeability of cosmetic ingredients. *Journal of Industrial and Engineering Chemistry* **2016**, *39*, 121–126.

169. Mönkäre, J.; Reza Nejadnik, M.; Baccouche, K.; Romeijn, S.; Jiskoot, W.; Bouwstra, J. A. IgG-loaded hyaluronan-based dissolving microneedles for intradermal protein delivery. *Journal of Controlled Release* **2015**, *218*, 53–62.

170. Marin, E.; Briceño, M. I.; Caballero-George, C. Critical evaluation of biodegradable polymers used in nanodrugs. *International Journal of Nanomedicine* **2013**, *8*, 3071–3091.

171. Nair, N. R.; Sekhar, V. C.; Nampoothiri, K. M.; Pandey, A. Biodegradation of Biopolymers. In *Current Developments in Biotechnology and Bioengineering: Production, Isolation and Purification of Industrial Products*; Elsevier, 2016; pp. 739–755.

172. Jin, J.; Reese, V.; Coler, R.; Carter, D.; Rolandi, M. Chitin Microneedles for an Easy-to-Use

Tuberculosis Skin Test. *Advanced Healthcare Materials* **2014**, *3*, 349–353.

173. Chen, M.-C. C.; Ling, M.-H. H.; Lai, K.-Y. Y.; Pramudityo, E. Chitosan microneedle patches for sustained transdermal delivery of macromolecules. *Biomacromolecules* **2012**, *13*, 4022–4031.

174. Justin, R.; Román, S.; Chen, D.; Tao, K.; Geng, X.; Grant, R. T.; MacNeil, S.; Sun, K.; Chen, B. Biodegradable and conductive chitosan–graphene quantum dot nanocomposite microneedles for delivery of both small and large molecular weight therapeutics. *RSC Advances* **2015**, *5*, 51934–51946.

175. Ling, M.-H. H.; Chen, M.-C. C. Dissolving polymer microneedle patches for rapid and efficient transdermal delivery of insulin to diabetic rats. *Acta Biomaterialia* **2013**, *9*, 8952–8961.

176. Stinson, J. A.; Raja, W. K.; Lee, S.; Kim, H. B.; Diwan, I.; Tutunjian, S.; Panilaitis, B.; Omenetto, F. G.; Tzipori, S.; Kaplan, D. L. Silk Fibroin Microneedles for Transdermal Vaccine Delivery. *ACS Biomaterials Science & Engineering* **2017**, *3*, acsbiomaterials.6b00515.

177. Eltayib, E.; Brady, A. J.; Caffarel-Salvador, E.; Gonzalez-Vazquez, P.; Zaid Alkilani, A.; McCarthy, H. O.; McElnay, J. C.; Donnelly, R. F. Hydrogel-forming microneedle arrays: Potential for use in minimally-invasive lithium monitoring. *European Journal of Pharmaceutics and Biopharmaceutics* **2016**, *102*, 123–131.

178. Yang, S.; Wu, F.; Liu, J.; Fan, G.; Welsh, W.; Zhu, H.; Jin, T. Phase-Transition Microneedle Patches for Efficient and Accurate Transdermal Delivery of Insulin. *Advanced Functional Materials* **2015**, *25*, 4633–4641.

179. Lee, K. Y.; Rowley, J. A.; Eiselt, P.; Moy, E. M.; Bouhadir, K. H.; Mooney, D. J. Controlling mechanical and swelling properties of alginate hydrogels independently by cross-linker type and cross-linking density. *Macromolecules* **2000**, *33*, 4291–4294.

180. Kim, Y.-C. C.; Park, J.-H. H.; Prausnitz, M. R. Microneedles for drug and vaccine delivery.

Advanced Drug Delivery Reviews **2012**, *64*, 1547–1568.

181. Vilela, C.; Pinto, R. J. B.; Pinto, S.; Marques, P. A. A. P.; Silvestre, A. J. D.; Freire, C. S. R. *Polysaccharide based hybrid materials*; SpringerBriefs in Molecular Science; Springer International Publishing: Cham, 2018.

182. Hiraishi, Y.; Nakagawa, T.; Quan, Y. S.; Kamiyama, F.; Hirobe, S.; Okada, N.; Nakagawa, S. Performance and characteristics evaluation of a sodium hyaluronate-based microneedle patch for a transcutaneous drug delivery system. *International Journal of Pharmaceutics* **2013**, *441*, 570–579.

183. Matsuo, K.; Yokota, Y.; Zhai, Y.; Quan, Y. S.; Kamiyama, F.; Mukai, Y.; Okada, N.; Nakagawa, S. A low-invasive and effective transcutaneous immunization system using a novel dissolving microneedle array for soluble and particulate antigens. *Journal of Controlled Release* **2012**, *161*, 10–17.

184. Liu, S.; Jin, M.; Quan, Y.; Kamiyama, F.; Katsumi, H.; Sakane, T.; Yamamoto, A. The development and characteristics of novel microneedle arrays fabricated from hyaluronic acid, and their application in the transdermal delivery of insulin. *Journal of Controlled Release* **2012**, *161*, 933–941.

185. Zhu, Z.; Ye, X.; Ku, Z.; Liu, Q.; Shen, C.; Luo, H.; Luan, H.; Zhang, C.; Tian, S.; Lim, C. Y.; Huang, Z.; Wang, H. Transcutaneous immunization via rapidly dissolvable microneedles protects against hand-foot-and-mouth disease caused by enterovirus 71. *Journal of Controlled Release* **2016**, *243*, 291–302.

186. Chen, M.-Y. M.-C.; Chen, Y.-Y.; Tsai, H.-T.; Tzai, T.-S.; Chen, M.-Y. M.-C.; Tsai, Y.-S. Transdermal Delivery of Luteinizing Hormone-releasing Hormone with Chitosan Microneedles: A Promising Tool for Androgen Deprivation Therapy. *Anticancer Research* **2017**, *37*, 6791–6797.

187. Justin, R.; Chen, B. Multifunctional chitosan–magnetic graphene quantum dot nanocomposites for the release of therapeutics from detachable and non-detachable biodegradable microneedle arrays. *Interface Focus* **2018**, *8*, 20170055.

188. Chen, M. C.; Lai, K. Y.; Ling, M. H.; Lin, C. W. Enhancing immunogenicity of antigens through sustained intradermal delivery using chitosan microneedles with a patch-dissolvable design. *Acta Biomaterialia* **2018**, *65*, 66–75.

189. Ito, Y.; Matsumoto, K.; Osakama, N.; Yoshioka, R.; Kobuchi, S.; Sakaeda, T.; Takada, K. Dissolving Microneedles as Skin Allergy Test Device. *Biological and Pharmaceutical Bulletin* **2017**, *40*, 531–534.

190. He, M.; Yang, G.; Zhang, S.; Zhao, X.; Gao, Y. Dissolving Microneedles Loaded With Etonogestrel Microcrystal Particles for Intradermal Sustained Delivery. *Journal of Pharmaceutical Sciences* **2018**, *107*, 1037–1045.

191. Park, Y. H.; Ha, S. K.; Choi, I.; Kim, K. S.; Park, J.; Choi, N.; Kim, B.; Sung, J. H. Fabrication of degradable carboxymethyl cellulose (CMC) microneedle with laser writing and replica molding process for enhancement of transdermal drug delivery. *Biotechnology and Bioprocess Engineering* **2016**, *21*, 110–118.

192. Hao, Y.; Chen, Y.; Lei, M.; Zhang, T.; Cao, Y.; Peng, J.; Chen, L.; Qian, Z. Near-Infrared Responsive PEGylated Gold Nanorod and Doxorubicin Loaded Dissolvable Hyaluronic Acid Microneedles for Human Epidermoid Cancer Therapy. *Advanced Therapeutics* **2018**, *1*, 1800008.

193. Nayak, A.; Das, D. B.; Vladisavljević, G. T. Microneedle-Assisted Permeation of Lidocaine Carboxymethylcellulose with Gelatine Co-polymer Hydrogel. *Pharmaceutical Research* **2014**, *31*, 1170–1184.

194. Yu, W.; Jiang, G.; Zhang, Y.; Liu, D.; Xu, B.; Zhou, J. Polymer microneedles fabricated from

alginate and hyaluronate for transdermal delivery of insulin. *Materials Science and Engineering C* **2017**, *80*, 187–196.

195. Chen, C. H.; Shyu, V. B. H.; Chen, C. T. Dissolving microneedle patches for transdermal insulin delivery in diabetic mice: Potential for clinical applications. *Materials* **2018**, *11*, 1625.

196. Park, S. Y.; Lee, H. U.; Lee, Y. C.; Kim, G. H.; Park, E. C.; Han, S. H.; Lee, J. G.; Choi, S.; Heo, N. S.; Kim, D. L.; Huh, Y. S.; Lee, J. Wound healing potential of antibacterial microneedles loaded with green tea extracts. *Materials Science and Engineering C* **2014**, *42*, 757–762.

197. Chen, F.; Yan, Q.; Yu, Y.; Wu, M. X. BCG vaccine powder-laden and dissolvable microneedle arrays for lesion-free vaccination. *Journal of Controlled Release* **2017**, *255*, 36–44.

198. World Health Organization *Recommendations to assure the quality , safety and efficacy of BCG vaccines*; 2011; Vol. 927.

199. Yan, X.; Lin, Y.; Jiang, Y.; Xu, Y.; Tan, Q. Adipose-derived SVFs with hyaluronic acid accelerate diabetic wound healing in diabetic porcine model. *Int J Clin Exp Med* **2018**, *11*, 735–740.

200. Dong, L.; Li, Y.; Li, Z.; Xu, N.; Liu, P.; Du, H.; Zhang, Y.; Huang, Y.; Zhu, J.; Ren, G.; Xie, J.; Wang, K.; Zhou, Y.; Shen, C.; Zhu, J.; Tao, J. Au Nanocage-Strengthened Dissolving Microneedles for Chemo-Photothermal Combined Therapy of Superficial Skin Tumors. *ACS Applied Materials and Interfaces* **2018**, *10*, 9247–9256.

201. Kim, S.; Lee, J.; Shayan, F. L.; Kim, S.; Huh, I.; Ma, Y.; Yang, H.; Kang, G.; Jung, H. Physicochemical study of ascorbic acid 2-glucoside loaded hyaluronic acid dissolving microneedles irradiated by electron beam and gamma ray. *Carbohydrate Polymers* **2018**, *180*, 297–303.

202. Larrañeta, E.; Henry, M.; Irwin, N. J.; Trotter, J.; Perminova, A. A.; Donnelly, R. F. Synthesis

and characterization of hyaluronic acid hydrogels crosslinked using a solvent-free process for potential biomedical applications. *Carbohydrate Polymers* **2018**, *181*, 1194–1205.

203. Bayarri, S.; González-Tomás, L.; Costell, E. Viscoelastic properties of aqueous and milk systems with carboxymethyl cellulose. *Food Hydrocolloids* **2009**, *23*, 441–450.

204. Dhar, N.; Akhlaghi, S. P.; Tam, K. C. Biodegradable and biocompatible polyampholyte microgels derived from chitosan, carboxymethyl cellulose and modified methyl cellulose. *Carbohydrate Polymers* **2012**, *87*, 101–109.

205. Kim, J. Y.; Han, M. R.; Kim, Y. H.; Shin, S. W.; Nam, S. Y.; Park, J. H. Tip-loaded dissolving microneedles for transdermal delivery of donepezil hydrochloride for treatment of Alzheimer's disease. *European Journal of Pharmaceutics and Biopharmaceutics* **2016**, *105*, 148–155.

206. Zaric, M.; Becker, P. D.; Hervouet, C.; Kalcheva, P.; Ibarzo Yus, B.; Cocita, C.; O'Neill, L. A.; Kwon, S. Y.; Klavinskis, L. S. Long-lived tissue resident HIV-1 specific memory CD8+T cells are generated by skin immunization with live virus vectored microneedle arrays. *Journal of Controlled Release* **2017**, *268*, 166–175.

207. Chen, H.-J.; Lin, D.; Liu, F.; Zhou, L.; Liu, D.; Lin, Z.; Yang, C.; Jin, Q.; Hang, T.; He, G.; Xie, X. Transdermal Delivery of Living and Biofunctional Probiotics through Dissolvable Microneedle Patches. *ACS Applied Bio Materials* **2018**, *1*, 374–381.

208. Fakhraei Lahiji, S.; Seo, S. H.; Kim, S.; Dangol, M.; Shim, J.; Li, C. G.; Ma, Y.; Lee, C.; Kang, G.; Yang, H.; Choi, K. Y.; Jung, H. Transcutaneous implantation of valproic acid-encapsulated dissolving microneedles induces hair regrowth. *Biomaterials* **2018**, *167*, 69–79.

209. Duarte, A. R. C.; Correlo, V. M.; Oliveira, J. M.; Reis, R. L. Recent Developments on Chitosan Applications in Regenerative Medicine. In *Biomaterials from Nature for Advanced Devices and Therapies*; John Wiley & Sons, Inc.: Hoboken, New Jersey, 2016; pp. 221–243.

210. Baldrick, P. The safety of chitosan as a pharmaceutical excipient. *Regulatory Toxicology and Pharmacology* **2010**, *56*, 290–299.

211. Wu, Q. X.; Lin, D. Q.; Yao, S. J. Design of chitosan and its water soluble derivatives-based drug carriers with polyelectrolyte complexes. *Marine Drugs* **2014**, *12*, 6236–6253.

212. Bellich, B.; D'Agostino, I.; Semeraro, S.; Gamini, A.; Cesàro, A. "The good, the bad and the ugly" of chitosans. *Marine Drugs* 2016, *14*.

213. Rodrigues, A.; Emeje, M. Recent applications of starch derivatives in nanodrug delivery. *Carbohydrate Polymers* **2012**, *87*, 987–994.

214. Torres, F.; Arce, D. Starch-Based Nanocomposites for Biomedical Applications. In *Biodegradable Polymeric Nanocomposites*; CRC Press, 2015; pp. 73–94.

215. Lee, I. C.; Lin, W. M.; Shu, J. C.; Tsai, S. W.; Chen, C. H.; Tsai, M. T. Formulation of two-layer dissolving polymeric microneedle patches for insulin transdermal delivery in diabetic mice. *Journal of Biomedical Materials Research - Part A* **2017**, *105*, 84–93.

216. Van Vlierberghe, S.; Graulus, G. J.; Samal, S. K.; Van Nieuwenhove, I.; Dubruel, P. Porous hydrogel biomedical foam scaffolds for tissue repair. In *Biomedical Foams for Tissue Engineering Applications*; Woodhead Publishing, 2014; pp. 335–390.

217. Edens, C.; Dybdahl-Sissoko, N. C.; Weldon, W. C.; Oberste, M. S.; Prausnitz, M. R. Inactivated polio vaccination using a microneedle patch is immunogenic in the rhesus macaque. *Vaccine* **2015**, *33*, 4683–4690.

218. Chen, B. Z.; Ashfaq, M.; Zhu, D. D.; Zhang, X. P.; Guo, X. D. Controlled Delivery of Insulin Using Rapidly Separating Microneedles Fabricated from Genipin-Crosslinked Gelatin. *Macromolecular Rapid Communications* **2018**.

219. Jin, H. J.; Kaplan, D. L. Mechanism of silk processing in insects and spiders. *Nature* **2003**,

424, 1057–1061.

220. Brown, J.; Lu, C. L.; Coburn, J.; Kaplan, D. L. Impact of silk biomaterial structure on proteolysis. *Acta Biomaterialia* **2015**, *11*, 212–221.

221. Cao, Y.; Wang, B. Biodegradation of silk biomaterials. *International Journal of Molecular Sciences* **2009**, *10*, 1514–1524.

222. Demuth, P. C.; Min, Y.; Irvine, D. J.; Hammond, P. T. Implantable silk composite microneedles for programmable vaccine release kinetics and enhanced immunogenicity in transcutaneous immunization. *Advanced Healthcare Materials* **2014**, *3*, 47–58.

223. Rieu, C.; Bertinetti, L.; Schuetz, R.; Salinas-Zavala, C. C.; Weaver, J. C.; Fratzl, P.; Miserez, A.; Masic, A. The role of water on the structure and mechanical properties of a thermoplastic natural block co-polymer from squid sucker ring teeth. *Bioinspiration and Biomimetics* **2016**, *11*, 055003.

224. Guerette, P. A.; Hoon, S.; Seow, Y.; Raida, M.; Masic, A.; Wong, F. T.; Ho, V. H. B.; Kong, K. W.; Demirel, M. C.; Pena-Francesch, A.; Amini, S.; Tay, G. Z.; Ding, D.; Miserez, A. Accelerating the design of biomimetic materials by integrating RNA-seq with proteomics and materials science. *Nature Biotechnology* **2013**, *31*, 908–915.

225. Demir, M.; Ramos-Rivera, L.; Silva, R.; Nazhat, S. N.; Boccaccini, A. R. Zein-based composites in biomedical applications. *Journal of Biomedical Materials Research - Part A* **2017**, *105*, 1656–1665.

226. Than, A.; Liang, K.; Xu, S.; Sun, L.; Duan, H.; Xi, F.; Xu, C.; Chen, P. Transdermal Delivery of Anti-Obesity Compounds to Subcutaneous Adipose Tissue with Polymeric Microneedle Patches. *Small Methods* **2017**, *1*, 1700269.

227. Kim, J. D.; Kim, M.; Yang, H.; Lee, K.; Jung, H. Droplet-born air blowing: Novel dissolving

microneedle fabrication. *Journal of Controlled Release* **2013**, *170*, 430–436.

228. Huh, I.; Kim, S.; Yang, H.; Jang, M.; Kang, G.; Jung, H. Effects of two droplet-based dissolving microneedle manufacturing methods on the activity of encapsulated epidermal growth factor and ascorbic acid. *European Journal of Pharmaceutical Sciences* **2018**, *114*, 285–292.

229. Fakhraei Lahiji, S.; Jang, Y.; Ma, Y.; Dangol, M.; Yang, H.; Jang, M.; Jung, H. Effects of dissolving microneedle fabrication parameters on the activity of encapsulated lysozyme. *European Journal of Pharmaceutical Sciences* **2018**, *117*, 290–296.

230. Yu, W.; Jiang, G.; Zhang, Y.; Liu, D.; Xu, B.; Zhou, J. Polymer microneedles fabricated from alginate and hyaluronate for transdermal delivery of insulin. *Materials Science and Engineering C* **2017**, *80*, 187–196.

231. Yao, G.; Quan, G.; Lin, S.; Peng, T.; Wang, Q.; Ran, H.; Chen, H.; Zhang, Q.; Wang, L.; Pan, X.; Wu, C. Novel dissolving microneedles for enhanced transdermal delivery of levonorgestrel: In vitro and in vivo characterization. *International Journal of Pharmaceutics* **2017**, *534*, 378–386.

232. Adikwu, M. U.; Esimone, C. O. *Biopolymers in Drug Delivery: Recent Advances and Challenges*; 2009.

233. ICH Annex 2 Stability testing of active pharmaceutical ingredients and fi nished pharmaceutical products. **2009**, 87–130.

234. Lee, S. G.; Jeong, J. H.; Lee, K. M.; Jeong, K. H.; Yang, H.; Kim, M.; Jung, H.; Lee, S.; Choi, Y. W. Nanostructured lipid carrier-loaded hyaluronic acid microneedles for controlled dermal delivery of a lipophilic molecule. *International Journal of Nanomedicine* **2013**, *9*, 289–299.

235. DeMuth, P. C.; Su, X.; Samuel, R. E.; Hammond, P. T.; Irvine, D. J. Nano-layered microneedles for transcutaneous delivery of polymer nanoparticles and plasmid DNA. *Advanced Materials* **2010**, *22*, 4851–4856.

236. Gupta, J.; Gill, H. S.; Andrews, S. N.; Prausnitz, M. R. Kinetics of skin resealing after insertion of microneedles in human subjects. *Journal of Controlled Release* **2011**, *154*, 148–155.

237. Martin, A.; McConville, A.; Anderson, A.; McLister, A.; Davis, J. Microneedle Manufacture: Assessing Hazards and Control Measures. *Safety* **2017**, *3*, 25.

Table captions

TABLE 1. ADVANTAGES AND DISADVANTAGES OF DISSOLVABLE, BIODEGRADABLE AND SWELLABLE POLYMERIC MICRONEEDLES [18].

TABLE 2. OVERVIEW OF POLYSACCHARIDE-BASED MNS FOR THE DELIVERY OF ACTIVE PHARMACEUTICAL INGREDIENTS.

TABLE 3. OVERVIEW OF PROTEIN-BASED MNS FOR THE DELIVERY OF ACTIVE PHARMACEUTICAL INGREDIENTS.

TABLE 4. FAILURE FORCE AFTER AN AXIAL FORCE LOAD OF POLYSACCHARIDE AND PROTEIN-BASED MICRONEEDLES.

Figure captions

Figure 1. Schematic representation of the side view of microneedles inserted into the skin.

Figure 2. Schematic illustration of microneedles. (A) Microneedle structure defined as (a) in-plane and (b) out-of-plane. (B) Shape defined as (a) hollow and (b) solid shape. (C) Geometry of needles defined as (a) cylindrical, (b) tapered tip, (c) conical, (d) pyramidal and (e) pentagonal-base canonical tip. Reproduced with permission from ref. 43 (Copyright © 2011, Molecular Diversity Preservation International).

FIGURE 3. CLASSIFICATION OF MICRONEEDLES ACCORDINGLY TO PATTERNS OF DRUG DELIVERY. (A) SOLID, (B) COATED, (C) DISSOLVING, (D) HOLLOW, (E) HYDROGEL-FORMING MICRONEEDLES [43].

Figure 4. Representative illustration of (a) conventional microfabrication technology. Reproduced with permission from ref.[99] (Copyright © 2016, Molecular Diversity Preservation International); (b) magnetic assembly process. Reproduced with permission from ref. [100] (Copyright © 2016, PLoS ONE); (c) general micromolding process. Reproduced with permission from ref. [100] (Copyright © 2017, Royal Society of Chemistry); (d) Droplet-based methods, namely droplet-born air blowing and centrifugal lithography. Reproduced with permission from ref. [61] (Copyright © 2018, Elsevier).

FIGURE 5. FORCE (N) VERSUS DISPLACEMENT CURVES OF MICRONEEDLES REGARDING (A) AXIAL FORCE TEST AND (B) TRANSVERSE FORCE TEST. REPRODUCED WITH PERMISSION FROM REF. [62] (COPYRIGHT © 2013, PLOS ONE).

FIGURE 6. SKIN PENETRATION VISUALIZATION USING (A) DYES; (B) HEMATOXYLIN EOSIN STAINING. REPRODUCED WITH PERMISSION FROM REF. [141] (COPYRIGHT © 2010, NATURE); AND (C) OPTICAL COHERENCE TOMOGRAPHY. REPRODUCED WITH PERMISSION FROM REF. [142] (COPYRIGHT © 2010, ELSEVIER).

FIGURE 7. BRIGHT FIELD MICROGRAPH OF 800 μM HYALURONIC ACID MICRONEEDLE ARRAYS (A) BEFORE SKIN INSERTION AND AFTER (B) 5 AND (C) 60 MINUTES. REPRODUCED WITH PERMISSION FROM REF. 182 (COPYRIGHT © 2012, ELSEVIER).

FIGURE 8. THREE-DIMENSIONAL IMAGES OF SIDE VIEW OF MICRONEEDLES OBTAINED BY TWO PHOTON CONFOCAL MICROSCOPY. (A) INTEGRAL MICRONEEDLE AT (B) TWO, (C) 7 AND (D) 19H AFTER INSERTION INTO SKIN. REPRODUCED WITH PERMISSION FROM REF. [203] (COPYRIGHT © 2017, ELSEVIER).

FIGURE 9. (A) SCHEMATIC REPRESENTATION OF MICRONEEDLES FOR SKIN TUMOR TREATMENT. (B) IN VIVO BIOLUMINESCENCE IMAGING OF THE TUMORS OF DIFFERENT GROUPS INDICATED (1, UNTREATED; 2, MN-GOX; 3, FREE APD1; 4, MN-APD1; 5, MN-GOX-APD1). (C) QUANTIFIED TUMOR SIGNALS ACCORDING TO KAPLAN - MEIER SURVIVAL CURVES FOR THE TREATED AND THE CONTROL MICE. SHOWN ARE EIGHT MICE PER TREATMENT GROUP. REPRODUCED WITH PERMISSION FROM REF. [85] (COPYRIGHT © 2016, AMERICAN CHEMICAL SOCIETY).

FIGURE 10. SWELLABLE MICRONEEDLES FABRICATED USING METHACRYLATED HYALURONIC ACID. (A) SCHEMATIC REPRESENTATION OF THE CROSS-LINKED NETWORK. (B) SWELLING BEHAVIOUR OF METHACRYLATED MICRONEEDLES WITH TIME. (C) CORRELATION OF THE REAL GLUCOSE CONCENTRATIONS IN HYDROGEL WITH THE CALCULATED VALUES BASED ON EXTRACTION AND THE RECOVERY USING 10 K RPM CENTRIFUGATION FOR 5 MIN. THE DOTS WERE FITTED AS LINE WITH R^2 = 0.98391. (D) CORRELATION OF THE REAL CHOLESTEROL CONCENTRATIONS IN HYDROGEL WITH THE CALCULATED VALUES BASED ON THE EXTRACTION AND THE RECOVERY USING 10 000 RPM CENTRIFUGATION FOR 5 MIN. THE DOTS WERE FITTED AS LINE WITH R^2= 0.98467. *P < 0.05. REPRODUCED WITH PERMISSION FROM REF. [85] (COPYRIGHT © 2017, WILEY).

FIGURE 11. SCHEMATIC REPRESENTATION OF MICRONEEDLES DELIVERING VALPROIC ACID. (B) FLUORESCENCE IMAGES OF VALPROIC ACID DELIVERY IN MICE. (C) PHOTOGRAPH OF HAIR REGROWTH IN MICE. REPRODUCED WITH PERMISSION FROM REF. [210] (COPYRIGHT © 2018, ELSEVIER).

FIGURE 12. CHITOSAN MNS WITH A DISSOLVABLE PEDESTAL FOR OVALBUMIN DELIVERY. (A) SCHEMATIC REPRESENTATION. (B) FLUORESCENCE MICROGRAPH OF THE FITC-MICRONEEDLES AFTER INSERTION. (C) OVALBUMIN-SPECIFIC LEVELS OF IGG AFTER ADMINISTRATION OF MICRONEEDLES. (D) IN VIVO SKIN RETENTION PROFILE OF OVALBUMIN. REPRODUCED WITH PERMISSION FROM REF. [189] (COPYRIGHT © 2013, ELSEVIER)

FIGURE 13. (A) GELATIN MICRONEEDLES BEFORE AND AFTER INSERTION INTO PIG SKIN. (B) SEROLOGIC RESPONSE AND NEUTRALIZING ANTIBODY TITERS TO POLIOVIRUS FOLLOWING VACCINATION. RHESUS MACAQUES WERE VACCINATED AT WEEK 0 AND WEEK 8 WITH IPV GIVEN EITHER BY MICRONEEDLE (MN) PATCH OR INTRAMUSCULAR (IM) INJECTION. SERUM WAS COLLECTED WEEKLY AND ANALYSED USING A SEROTYPE-SPECIFIC MICRO-NEUTRALIZATION ASSAY. EACH DATA POINT REPRESENTS A SINGLE ANIMAL WHILE THE LINES REPRESENT THE MEDIAN OF EACH GROUP. REPRODUCED WITH PERMISSION FROM REF. [231] (COPYRIGHT © 2015, ELSEVIER).

FIGURE 14. (A) GELATIN MICRONEEDLES BEFORE AND AFTER INSERTION INTO PIG SKIN. (B) SEROLOGIC RESPONSE AND NEUTRALIZING ANTIBODY TITERS TO POLIOVIRUS FOLLOWING VACCINATION. RHESUS MACAQUES WERE VACCINATED AT WEEK 0 AND WEEK 8 WITH IPV GIVEN EITHER BY MICRONEEDLE (MN) PATCH OR INTRAMUSCULAR (IM) INJECTION. SERUM WAS COLLECTED WEEKLY AND ANALYSED USING A SEROTYPE-SPECIFIC MICRO-NEUTRALIZATION ASSAY. EACH DATA POINT REPRESENTS A SINGLE ANIMAL WHILE THE LINES REPRESENT THE MEDIAN OF EACH GROUP. REPRODUCED WITH PERMISSION FROM REF. [231] (COPYRIGHT © 2015, ELSEVIER).

FIGURE 15. EFFICIENCY OF SUCKERIN MICRONEEDLES IN DRUG DELIVERY. (A) HAEMATOXYLIN-EOSIN STAINING OF RAT SKIN SHOWING SKIN BREAKAGE (ARROWS) AFTER PENETRATION. (B) MECHANICAL PROPERTIES OF SUCKERIN MICRONEEDLES IN DIFFERENT CONDITIONS OBTAINED. (C) ACCUMULATIVE RELEASE PROFILES OF RHODAMINE B

from sucKerin microneedles under different conditions. (d) Photograph of inhibition of *E. coli* exposed to kanamycin-loaded sucKerin microneedles. Reproduced with permission from ref. [71] (Copyright © 2017, Royal Society of Chemistry).

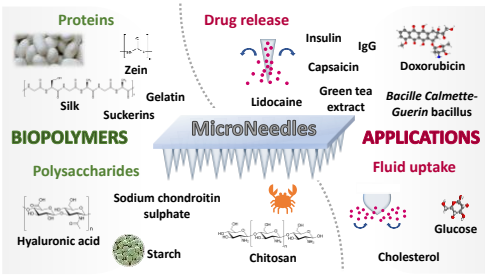

Graphical abstract

TABLE 1. ADVANTAGES AND DISADVANTAGES OF DISSOLVABLE, BIODEGRADABLE AND SWELLABLE POLYMERIC MICRONEEDLES [18].

MICRONEEDLES	ADVANTAGES	DISADVANTAGES
DISSOLVABLE	DISSOLVES WITHIN SHORT PERIODS ALLOWING A FAST DRUG RELEASE INCREASED DRUG LOADING BY ENCAPSULATION OR COATING PRECISE DRUG LOADING	PATIENTS NEED TO WAIT FOR COMPLETE DISSOLUTION BEFORE REMOVING THE PATCH
BIODEGRADABLE	USUALLY EMPLOYED FOR SUSTAINED DRUG RELEASE INCREASED DRUG LOADING BY ENCAPSULATION OR COATING PRECISE DRUG LOADING	POLYMER RESIDUES CAN BE DETECTED IN SKIN AFTER FEW DAYS
SWELLABLE	ALLOWS ATTACHMENT OF DRUG RESERVOIR INTACT REMOVAL OF SKIN SOFTNESS PRECLUDES REINSERTION AFTER REMOVAL LEAVES NO MEASURABLE POLYMER RESIDUE BEHIND TREATMENT CAN BE STOPPED IF NECESSARY	LIMITED DRUG LOADING INTO THE POLYMERIC MATRIX CROSS-LINKING CONDITIONS MAY AFFECT BIOACTIVITY OF DRUGS

TABLE 2. OVERVIEW OF POLYSACCHARIDE-BASED MNS FOR THE DELIVERY OF ACTIVE PHARMACEUTICAL INGREDIENTS.

BIOPOLYMER(S)	OTHER COMPONENTS	PHARMACEUTICAL INGREDIENT	OUTCOME	REFERENCE
HYALURONIC ACID		ALL-*TRANS* RETINOIC ACID, OVALBUMIN, TETANUS TOXOID- AND DIPHTHERIA TOXOID	GOOD STABILITY OF MICRONEEDLES; STORAGE FOR 12 MONTHS INDUCED IMMUNOLOGICAL RESPONSES.	[183]

	Ovalbumin and adenovirus vector	Immunization comparable to the conventional vaccination; improved responses to every soluble antigen like toxoids.	[184]
	Fluorescein isothiocyanate-dexiran	Increased permeation of high molecular weight drugs.	[198]
	Insulin	Dose-dependent hypoglycemic effect, similar to subcutaneous insulin injection.	[185]
	Green tea exiract	Reduction of bacterial growth (95%) on wound infected sites, for both gram negative and positive bacteria.	[197]
	Enterovirus 71 virus-like particles	Immunization induced high levels of antibody responses, comparable to intramuscular injection; enterovirus remained stable during fabrication and conferred protection against hand-foot-and-mouth disease.	[186]
Nanostructured lipid carriers using compritol, labrafil	Nile red	Successful delivery systiem	[199]

		FOR LIPOPHILIC COMPOUNDS.	
	IGG (IMMUNOGLOBULIN G)	PROTEIN INTEGRITY WAS PRESERVED WITH MORE THAN 80% RECOVERED AND ITS TERTIARY STRUCTURE UNALTERED.	[170]
AMYLOPECTIN	NIACINAMIDE AND ASCORBIC ACID	POTENTIAL TO BE USED IN COSMETICS DUE TO ITS ANTI-OXIDANT ACTIVITY.	[169]
	TUBERCULIN PURIFIED DERIVATIVES	INDUCED AN IMMUNE RESPONSE; USEFUL IN TUBERCULOSIS DIAGNOSIS.	[127]
	ADENOSINE	DISPLAYED BETTER OR COMPARABLE RESULTS RELATIVE TO CREAM APPLICATION.	[148]
	ADENOSINE	IMPROVED FACIAL WRINKLES WHEN COMBINED WITH CREAM.	[200]
AU NANOCAGES LOADED WITH DRUG	DOXORUBICIN	PHOTOTHERMAL EFFECT OF AU NANOCAGES COUPLED WITH DOXORUBICIN ALLOWED TUMOR DESTRUCTION; EFFICIENT FOR SUPERFICIAL SKIN TUMORS.	[201]
	DERMATOPHAGOIDS FARINAE EXTRACT	USEFUL AS ALLERGEN-SPECIFIC	[202]

			IMMUNOTHERAPY METHOD.	
		LIVE ATTENUATED *BACILLE CALMETTE-GUERIN* BACILLUS	VACCINATION EFFECTS COMPARABLE TO CONVENTIONAL INJECTIONS; TECHNOLOGY ALLOWS DELIVERY OF VACCINE POWDERS.	[203]
		β-3-ADRENOCEPTOR AGONIST AND THYROID HORMONE	β-3-ADRENOCEPTOR AND THYROID HORMONE PROMOTED WHITE ADIPOSE TISSUE BROWNING AND SUPPRESSED GAIN OF BODY FAT AND WEIGHT IN OBESE MOUSE MODELS.	[204]
		PEGYLATED GOLD NANOROD AND DOXORUBICIN	GOOD CELL INHIBITION IN EPIDERMOID CANCER THERAPY. THE PHOTOTHERMAL EFFECT DESTROYED COMPLETELY A431 CELLS *IN VITRO*.	[193]
		ASCORBIC ACID 2-GLUCOSIDE	STERILITY USING E-BEAM IRRADIATION MAINTAINED THE DOSE AND ACTIVITY OF THE DRUG WITHOUT AFFECTING THE DISSOLUTION ABILITY AND DRUG RELEASE IN ITS FINAL PACKAGING.	[205]
HYALURONIC ACID AND CARBOXYMETHYL CELLULOSE	AMYLOPECTIN	RHODAMINE B	INCREASED RHODAMINE PERMEABILITY.	[154]

	Amylopectin	Rhodamine B Niacinamide	Improved permeability and can be useful for cosmetic purposes.	[154]
Hyaluronic acid + 3-aminophenylboronic acid-modified alginate		Insulin	Insulin retained pharmacological activity; induction a sustained hypoglycemic effect in diabetic mice.	[195]
Hyaluronic acid cross-linked with *N,N'*-methylenebis(acrylamide)	Nanoparticles of dexiran loaded with glucose oxidase and anti-PD1 antibodies	Anti-PD1 immunotherapy	Robust immune response in a single-administration in a melanoma using a mouse model; higher inhibition of tumor growth when compared to intratumor injection.	[85]
Sodium chondroitin sulphate	Poly(vinyl pyrrolidone), lyotropic liquid crystal systems	Sinomenine hydrochloride	Improved permeation of drug with sustained release for potential application on adjuvant arthritis model rats.	[206]
		Capsaicin	Pharmacological activity, measured by skin idiospasm, comparable of topical administration; microneedles can exert a rapid local analgesic action.	[207]

		Insulin	Good dose-dependency for the plasma glucose level; maximum hypoglycemic effect of insulin observed at 1.7 ± 0.2 h for the fully-loaded tip and 1.5 ± 0.2 h for the partially loaded tip.	[208]
Carboxymethyl cellulose		Recombinant human adenovirus type 5 vector encoding HIV-1 gag	Induces generation of long-lived antigen -specific cells at the mucosal surfaces, to exert local immunosurveillance and provide a frontline defense against pathogens.	[209]
		Valproic acid	Induces hair regrowth with higher accuracy when compared with topical formulations.	[210]
		(Anti-TNF-alpha-Ab)-HA conjugates	MNs can be used with applicable release profiles, to locally treat a broad range of inflammatory skin diseases.	[211]
	Amylopectin	Rhodamine B Ascorbic acid	Improvement of 3-fold permeability of rhodamine B and six-fold increase	[67]

			OF ASCORBIC ACID ANTIOXIDANT ACTIVITY, WHEN COMPARED TO TOPICAL ADMINISTRATION.	
	DOUBLE HYDROXIDES NANOPARTICLES	OVALBUMIN	SIGNIFICANTLY STRONG ANTIBODY RESPONSE WAS DETECTED, HIGHER THAN WITH SUBCUTANEOUS INJECTION.	[212]
		LACTOBACILLUS	FAST DISSOLUTION WITH NO LOCAL TISSUE IRRITATION; *LACTOBACILLUS* WERE FUNCTIONALLY BIOACTIVE *IN VIVO* AS PROVED BY THE DETECTED LACTIC ACID IN PIG AND RAT SKIN.	[213]
HYDROXYPROPYL METHYL CELLULOSE	CARBOXYMETHYL CELLULOSE	DONEPEZIL HYDROCHLORIDE	THE EFFICIENCY OF DRUG ADMINISTRATION USING MNS WAS MORE EFFECTIVE THAN VIA ORAL ROUTE; THESE MNS COULD REPLACE THE CURRENT TREATMENT OF ALZHEIMER'S DISEASE.	[214]
	POLY(VINYL ALCOHOL) AS BACK LAYER	ETONOGESTREL MICROCRYSTAL PARTICLES	ETONOGESTREL ENCAPSULATED IN THE TIPS OF MNS HAS NO EFFECT ON MECHANICAL PROPERTIES AND ENABLED ACHIEVING STEADIER PLASMA	[191]

			LEVEL OF HORMONE COMPARED WITH INTRADERMAL INJECTION	
	POLY(METHYLVINYLETHER CO-MALEIC ANHYDRIDE)	LIDOCAINE HYDROCHLORIDE	FAST ONSET TIME (<5 MIN) WHEN COMPARED WITH CREAM THAT HAD AN ONSET TIME FOR 100 MIN BUT LOWER EFFICACY (COMMERCIALLY AVAILABLE ANESTHESIA CREAM COULD LAST FOR ABOUT 130 MIN); STABLE FOR 3 MONTHS UNDER 40 ± 2 °C AND A HUMIDITY OF 75 ± 5%.	[215]
CHITIN		PURIFIED PROTEIN DERIVATIVE, CONTAINING A MIXTURE OF ANTIGENS	POSITIVE TESTS CONFIRM THE POTENTIAL OF USING CHITIN MNS AS A DIAGNOSTIC TOOL.	[173]
CHITOSAN	TREHALOSE, POLY(VINYL PYRROLIDONE)/POLY(VINYL ALCOHOL) AS SUPPORTING SYSTEM	LUTEINIZING HORMONE RELEASING HORMONE ANALOGS, GOSERELIN	FEASIBLE SYSTEM FOR DELIVERY OF ANDROGEN-DEPRIVATION THERAPY; A CASIRATION LEVEL WAS MAINTAINED FOR 2 WEEKS.	[187]
	β-SODIUM GLYCEROPHOSPHATE AND HYDROXYPROPYL β-CYCLODEXTRIN	LEVONORGESTREL	SIMILAR PHARMACOKINETIC PROFILE WHEN COMPARED TO ORAL ADMINISTRATION, WITH MORE CONSISTENT PLASMA LEVELS.	[216]

	Poly(vinyl alcohol) + Polyvinylpyrrolidone as supporting array	Ovalbumin	Administration of low-dose ovalbumin (200 μg) into rats induced a higher immunization than intramuscular injection of full dose (500 μg); high antibody levels were observed for 18 days.	[189]
	Magnetic graphene quantum dots + Polyethylene glycol	Lidocaine hydrochloride	Iontophoretic type array; increased drug release from 25.7% to 96.4% using electrical stimulation.	[188]
		Bovine serum albumin	Sustained release for atleast 8 days.	[176]
Starch	gelatin	Insulin	Significant hypoglycemic effect, delivering the entire payload within 5 min.	[176]
Hydroxyethyl starch (tips)	sodium chondroitin sulphate (needle structure)	Hepatitis B surface antigen (tips)	Same level of immunogenicity as a commercial vaccine; antigenicity was retained at 37 and 45 °C and only a 10% loss was observed after 6 months at 50 °C.	[217]
Dextran		Poly-L-arginine	Dose-dependent immunoreaction; proposed as an	[190]

		alternative skin allergy device.

Table 3. Overview of protein-based MNs for the delivery of active pharmaceutical ingredients

Biopolymer(s)	Other components	Pharmaceutical ingredient	Outcome	Reference
Gelatin			Reduction of subcutaneous fat at the site of MNs application; promotion of lipolysis and inhibiting lipogenesis.	[69]
	Calcium sulphate	Insulin	More sustained hypoglycemic effect when compared with subcutaneous injection.	[39]
	Carboxymethyl cellulose	Insulin	Relative pharmacologic availability and relative bioavailability of insulin was 95.6 and 85.7%, satisfactory when compared with traditional injection.	[230]
	Carboxymethyl cellulose as back layer	Insulin	Gradual and moderate decrease of blood glucose levels.	[196]
	Sucrose	Inactivated polio vaccine	Vaccination of rhesus macaques induced a weaker serological response when compared to IM but with potential do eradicate poliomyelitis.	[231]

	α-calcium hemihydrate	Clonidine hydrochloride	Released of 55% of drug at a constant rate during the first 4h.	[232]
Gelatin cross-linked using genipin	Poly(vinyl alcohol)-coated poly(lactic acid) (supporting pedestal)	Insulin	Controlled release of insulin. The degree of cross-linking enhances the mechanical strength as well as humidity resistance.	[233]
Silk fibroin	2-Ethoxyethanol	Fluorescein isothiocyanate - dextran	Swellable system displaying 2-10 times higher transdermal delivery than films with identical drug loading.	[152]
	Poly(vinyl alcohol) (supporting pedestal)	Insulin	Hypoglycemic effect with a maximum decrease in blood glucose levels of 64%, against the 54% achieved by injection.	[63]
		Vaccines against influenza, *Clostridium difficile*, and *Shigella*	Provided evidence for dose sparing since the actual dose was lower than the coated dose.	[177]
		Rhodamine B	Prolonged drug release up to 8 days.	[151]
Fish scale biopolymer (mainly collagen) + cellulose nanocrystals		Lidocaine hydrochloride	Successful transdermal administration with drug permeation rate increasing from 2.5 to 7.5% after 36 h.	[149]
Suckerins		Kanamycin	Efficient anti-bacterial activity, due to intrinsic antibiotic activity of suckerins coupled with kanamycin.	[71]

Zein	Ovalbumin	Lower bacterial peneiration compared with hypodermic injection. Coated ovalbumin was stable under storage at ambient and refrigerator conditions.	[70]
	Tamoxifen Gemcitabine	Coating of MNs results in greater deposition for tamoxifen; the poke-and-patch approach provided greater permeation for gemcitabine.	[234]

Table 4. Failure force after an axial force load of polysaccharide and protein-based microneedles.

Microneedle composition	Failure force (N/needle) or maximum withstanding force	Reference
Hyaluronic acid	> 0.05	[226]
Hyaluronic acid	0.4-0.6	[227]
Hyaluronic acid	≈0.28	[182]
Sodium alginate	0.18 Transverse force failure 0.04	[62]
Cy5-loaded Hyaluronic acid	> 0.05	[226]
Epidermal growth factor-loaded-hyaluronic acid	0.63-0.78	[228]
Enterovirus particles loaded-sodium hyaluronate	>0.08	[185]
Ascorbic acid loaded-hyaluronic acid	0.059-0.161	[228]
Lysozyme loaded-hyaluronic acid	0.20	[229]
Hyaluronic acid cross-linked with *N,N'*-methylenebis(acrylamide) loaded with dextran nanoparticles	0.38	[85]

3-aminophenylboronic acid-modified alginate and hyaluronate cross-linked with calcium and loaded with insulin	0.37	[230]
Methacrylated hyaluronic acid	>0.15	[38]
Gelatin and calcium sulphate	0.4	[39]
Bullet shaped-gelatin	≈0.3	[69]
Conical shaped-gelatin	≈0.15	[69]
Chitosan	>0.2	[173]
Chitosan–magnetic graphene quantum dot	>0.16	[187]
Dexiran with chitosan and beta-sodium glycerophosphate	Bearing pressure 60N	[231]
Dexiran	Bearing pressure 90N	[231]
Carboxymethyl celllose	0.5-0.8	[227]
Fish scale biopolymer	≈0.12	[166]
Silk	24-54 g/needle	[150]
Silk before treatment	0.225	[7]
After water vapor treatment	0.175	
Zein	0.45	[70]
Albumin-coated zein	0.53	

Figures

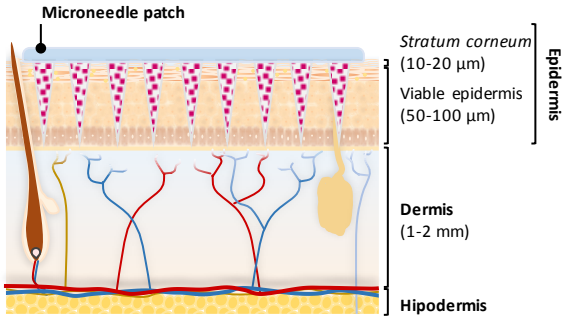

Figure 1. Schematic representation of the side view of microneedles inserted into the skin.

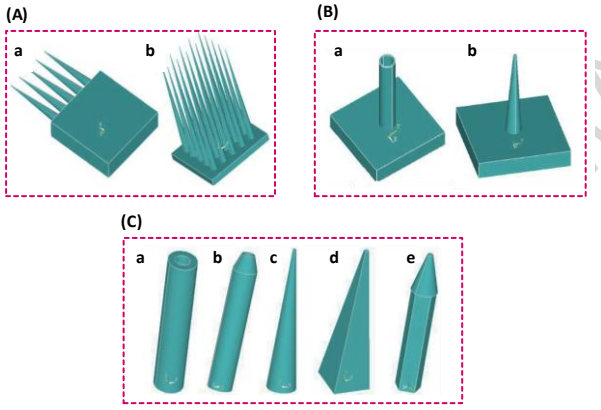

Figure 2. Schematic illustration of microneedles. (A) Microneedle structure defined as (a) in-plane and (b) out-of-plane. (B) Shape defined as (a) hollow and (b) solid shape. (C) Geometry of needles defined as (a) cylindrical, (b) tapered tip, (c) conical, (d) pyramidal and (e) pentagonal-base canonical tip. Reproduced with permission from ref. 43 (Copyright © 2011, Molecular Diversity Preservation International).

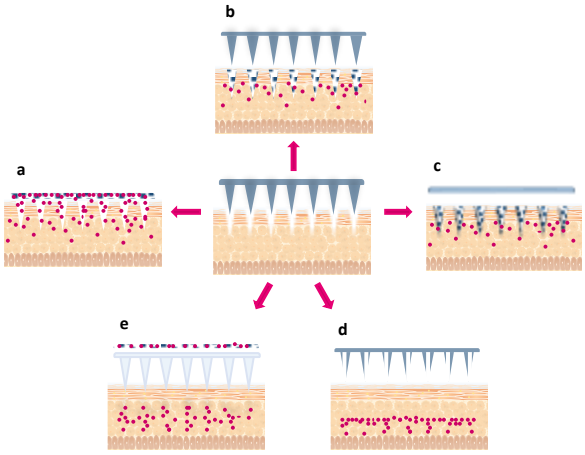

Figure 3. Classification of microneedles accordingly to patterns of drug delivery. (a) solid, (b) coated, (c) dissolving, (d) hollow, (e) hydrogel-forming microneedles [43].

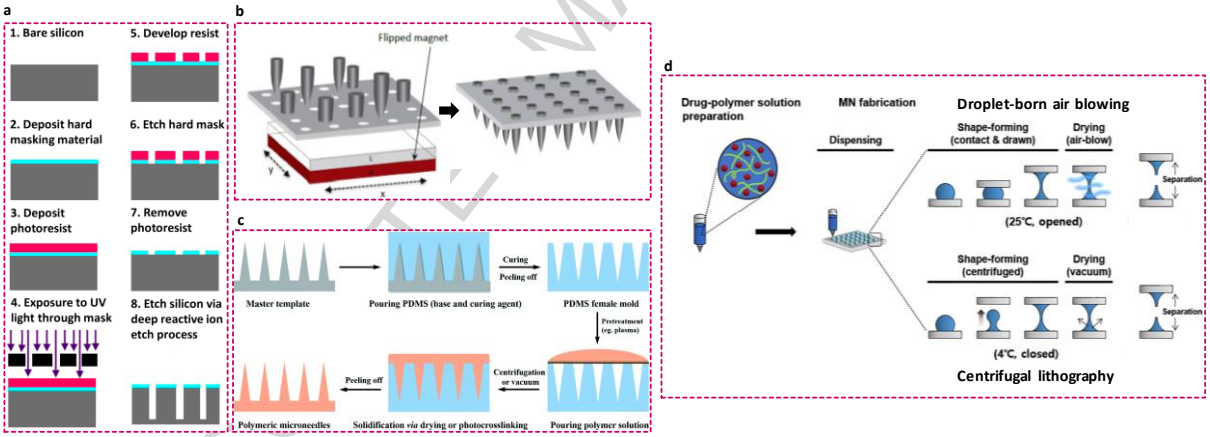

Figure 4. Representative illustration of (a) conventional microfabrication technology. Reproduced with permission from ref.[99] (Copyright © 2016, Molecular Diversity Preservation International); (b) magnetic assembly process. Reproduced with permission from ref. [100] (Copyright © 2016, PLoS ONE); (c) general micromolding process. Reproduced with permission from ref. [100] (Copyright © 2017, Royal Society of Chemistry); (d) Droplet-based methods,

namely droplet-born air blowing and centrifugal lithography. Reproduced with permission from ref. [61] (Copyright © 2018, Elsevier).

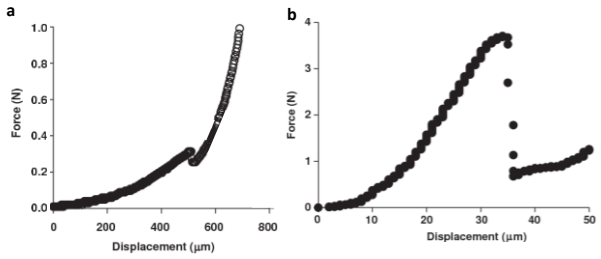

Figure 5. Force (N) versus displacement curves of microneedles regarding (a) axial force test and (b) transverse force test. Reproduced with permission from ref. [62] (Copyright © 2013, Plos one).

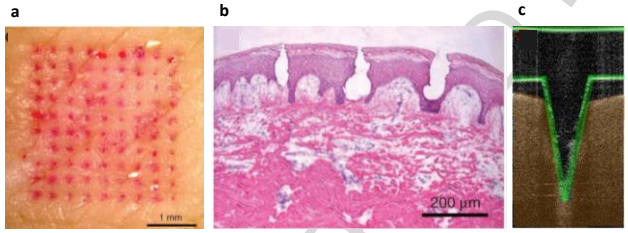

Figure 6. Skin penetration visualization using (a) dyes; (b) hematoxylin eosin staining. Reproduced with permission from ref. [141] (Copyright © 2010, Nature); and (c) optical coherence tomography. Reproduced with permission from ref. [142] (Copyright © 2010, Elsevier).

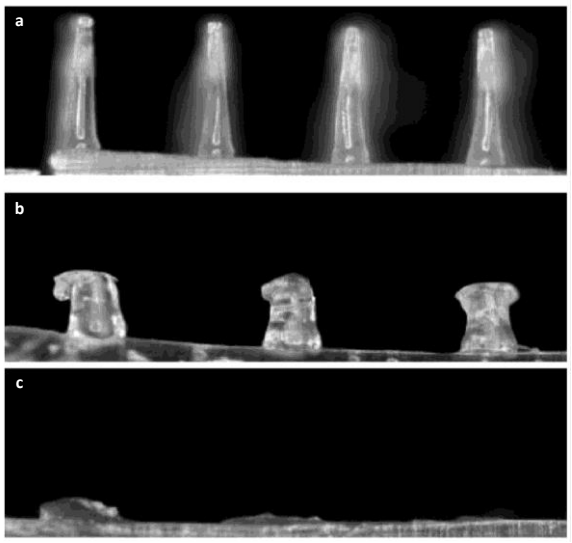

Figure 7. Bright field micrograph of 800 μm hyaluronic acid microneedle arrays (a) before skin insertion and after (b) 5 and (c) 60 minutes. Reproduced with permission from ref. 182 (Copyright © 2012, Elsevier).

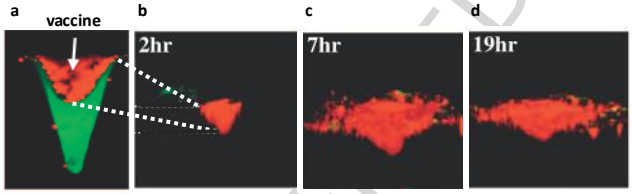

Figure 8. Three-dimensional images of side view of microneedles obtained by two photon confocal microscopy. (a) Integral microneedle at (b) two, (c) 7 and (d) 19h after insertion into skin. Reproduced with permission from ref. [203] (Copyright © 2017, Elsevier).

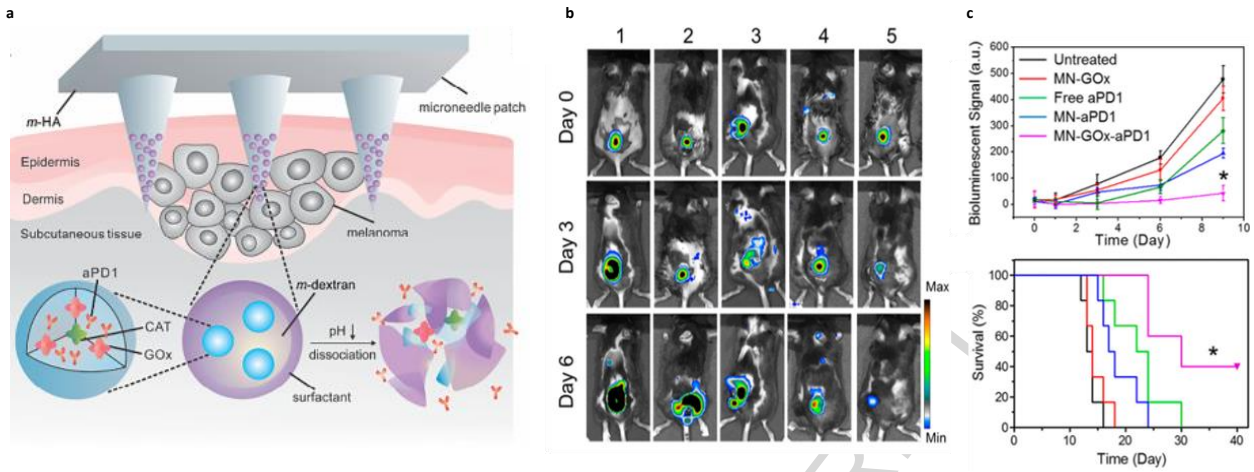

Figure 9. (a) Schematic representation of microneedles for skin tumor treatment. (b) In vivo bioluminescence imaging of the tumors of different groups indicated (1, untreated; 2, MN-GOx; 3, free aPD1; 4, MN-aPD1; 5, MN-GOx-aPD1). (c) Quantified tumor signals according to Kaplan - Meier survival curves for the treated and the control mice. Shown are eight mice per treatment group. Reproduced with permission from ref. [85] (Copyright © 2016, American Chemical Society.)

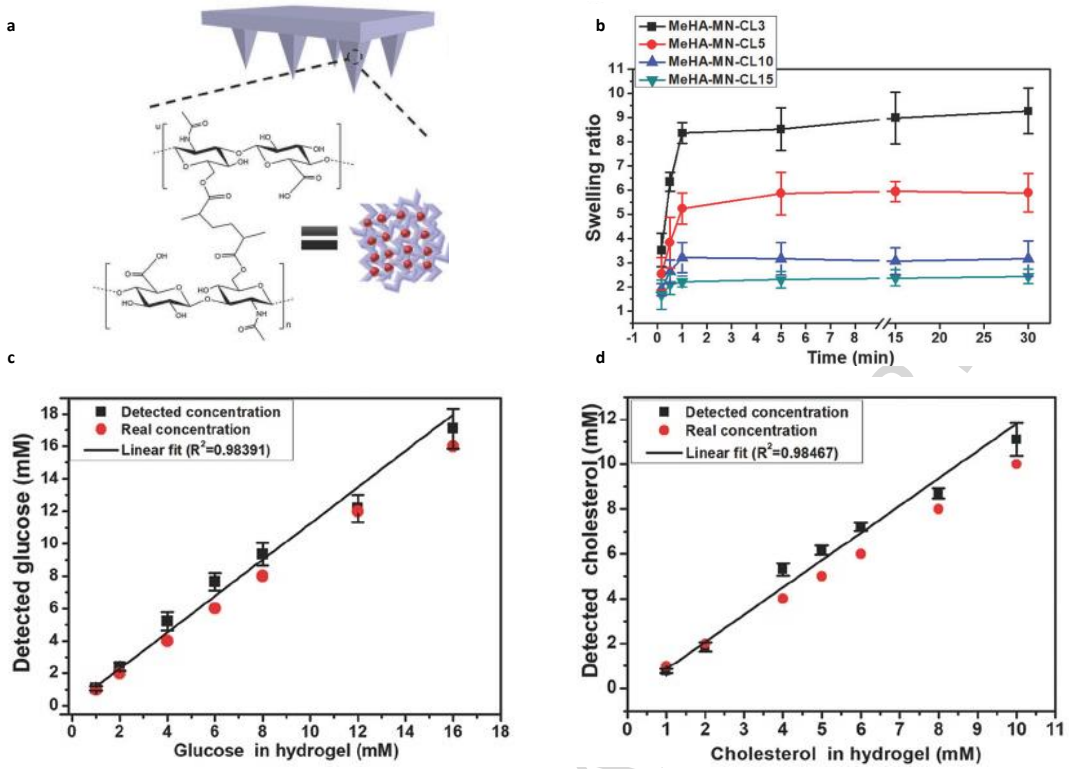

Figure 10. Swellable microneedles fabricated using methacrylated hyaluronic acid. (a) Schematic representation of the cross-linked network. (b) Swelling behaviour of methacrylated microneedles with time. (c) Correlation of the real glucose concentrations in hydrogel with the calculated values based on extraction and the recovery using 10 k rpm centrifugation for 5 min. The dots were fitted as line with R^2 = 0.98391. (d) Correlation of the real cholesterol concentrations in hydrogel with the calculated values based on the extraction and the recovery using 10 000 rpm centrifugation for 5 min. The dots were fitted as line with R^2= 0.98467. *P < 0.05. Reproduced with permission from ref. [85] (Copyright © 2017, Wiley).

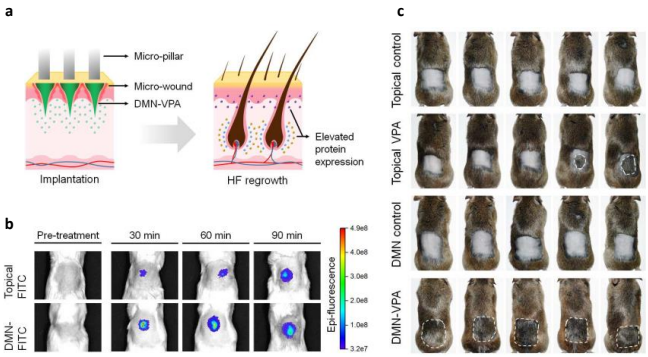

Figure 11. Schematic representation of microneedles delivering valproic acid. (b) Fluorescence images of valproic acid delivery in mice. (c) Photograph of hair regrowth in mice. Reproduced with permission from ref. [210] (Copyright © 2018, Elsevier).

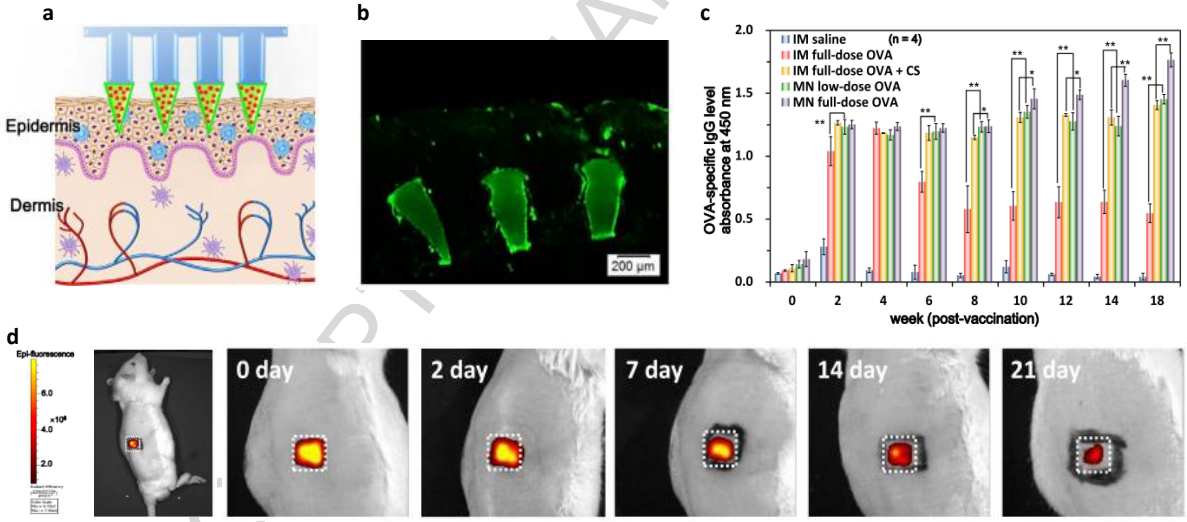

Figure 12. Chitosan MNs with a dissolvable pedestal for ovalbumin delivery. (a) Schematic representation. (b) Fluorescence micrograph of the FITC-microneedles after insertion. (c) Ovalbumin-specific levels of IgG after administration of microneedles. (d) In vivo skin retention profile of ovalbumin. Reproduced with permission from ref. [189] (Copyright © 2013, Elsevier).

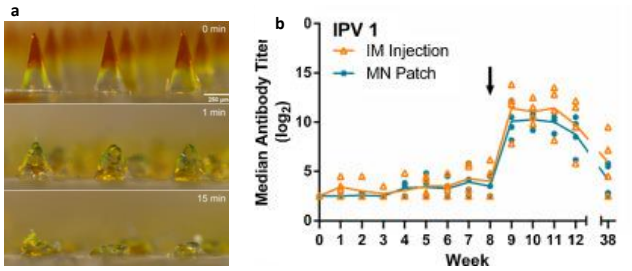

Figure 13. (a) Gelatin microneedles before and after insertion into pig skin. (b) Serologic response and neutralizing antibody titers to poliovirus following vaccination. Rhesus macaques were vaccinated at week 0 and week 8 with IPV given either by microneedle (MN) patch or intramuscular (IM) injection. Serum was collected weekly and analysed using a serotype-specific micro-neutralization assay. Each data point represents a single animal while the lines represent the median of each group. Reproduced with permission from ref. [231] (Copyright © 2015, Elsevier).

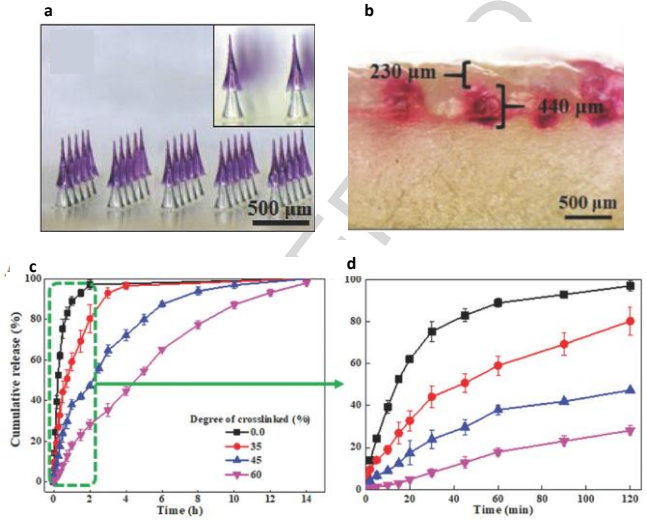

Figure 14. (a) Gelatin microneedles before and after insertion into pig skin. (b) Serologic response and neutralizing antibody titers to poliovirus following vaccination. Rhesus macaques were vaccinated at week 0 and week 8 with IPV given either by microneedle (MN) patch or

intramuscular (IM) injection. Serum was collected weekly and analysed using a serotype-specific micro-neutralization assay. Each data point represents a single animal while the lines represent the median of each group. Reproduced with permission from ref. [231] (Copyright © 2015, Elsevier).

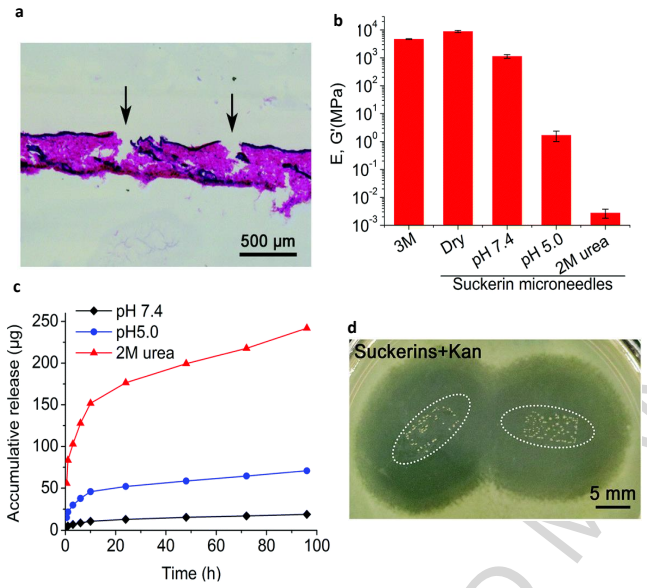

Figure 15. Efficiency of suckerin microneedles in drug delivery. (a) Haematoxylin-eosin staining of rat skin showing skin breakage (arrows) after penetration. (b) Mechanical properties of suckerin microneedles in different conditions obtained. (c) Accumulative release profiles of rhodamine B from suckerin microneedles under different conditions. (d) Photograph of inhibition of *E. coli* exposed to kanamycin-loaded suckerin microneedles. Reproduced with permission from ref. [71] (Copyright © 2017, Royal Society of Chemistry).